

# Constraints on QSO models from a relation between the QSO luminosity function and the local black hole mass function

Qingjuan Yu<sup>1,3</sup> and Youjun Lu<sup>1,2,3</sup>

<sup>1</sup>Canadian Institute for Theoretical Astrophysics, 60 St. George Street, Toronto, Ontario M5S 3H8, Canada

<sup>2</sup>Center for Astrophysics, University of Science and Technology of China, 96 Jinzhai Road, Hefei, Anhui 230026, P. R. China

## ABSTRACT

QSOs are believed to be powered by accretion onto massive black holes (BHs). In this paper, assuming that each central BH in nearby galaxies has experienced the QSO phase and ignoring BH mergers, we establish a relation between the QSO luminosity function (LF) and the local BH mass function (MF). The QSOLF is jointly controlled by the luminosity evolution of individual QSOs and the triggering history of the accretion onto seed BHs. By comparing the time integral of the QSOLF with that inferred from local BHs, we separate the effect of the luminosity evolution of individual QSOs from the effect of the triggering history. Assuming that the nuclear luminosity evolution includes two phases (first increasing at the Eddington luminosity with growth of BHs and then declining), we find that observations are generally consistent with the expected relation between the QSOLF and the local BHMF and obtain the following constraints on QSO models and BH growth: (i) The QSO mass-to-energy efficiency  $\epsilon$  should be  $\gtrsim 0.1$ . (ii) The lifetime (defined directly through the luminosity evolution of individual QSOs here) should be  $\gtrsim 4 \times 10^7$  yr. The characteristic declining timescale in the second phase should be significantly shorter than the Salpeter timescale  $\tau_{\text{Sp}}$ , and BH growth should not be dominated by the second phase. (iii) The ratio of obscured QSOs/AGNs to optically bright QSOs should be not larger than 7 at  $M_B \sim -23$  and 3 at  $M_B \sim -26$  if  $\epsilon = 0.31$ , and not larger than 1 at  $M_B \sim -23$  and negligible at  $M_B \sim -26$  if  $\epsilon = 0.1$ . (iv) It is unlikely that most QSOs are accreting at super-Eddington luminosities. We point out that it is hard to accurately estimate the value of the QSO lifetime estimated from the QSOLF and/or the local BHMF, if it is longer than a certain value (e.g.,  $\sim 4\tau_{\text{Sp}}$  in this study). We discuss the importance of accurate measurements of the intrinsic scatter in the BH mass and velocity dispersion relation of local galaxies and the scatter in the bolometric correction of QSOs. We also discuss some possible applications of the work in this paper, such as to the study of the demography of QSOs and the demography of normal galaxies at intermediate redshift.

*Subject headings:* black hole physics – galaxies: active – galaxies: evolution – galaxies: luminosity function, mass function – galaxies: nuclei – quasars: general

## 1. Introduction

The exploration of the relation of QSOs with massive black holes (BHs) in nearby galaxies has been of considerable interests since the discovery of QSOs. On the one hand, QSOs are suggested to be powered

---

<sup>3</sup>Current address: Astronomy Department, University of California at Berkeley, Berkeley, CA 94720, USA;  
Email: yqj@astro.berkeley.edu (QY); lyj@astro.berkeley.edu (YL)

by gas accretion onto massive BHs (Salpeter 1964; Zel’dovich & Novikov 1964). This (currently widely accepted) model suggests that a population of massive BHs as “dead” QSOs exist in nearby galactic centers (Lynden-Bell 1969). Furthermore, the total mass density of these remnant BHs and the typical BH mass in nearby galaxies can be inferred from the total energy density radiated in photons by QSOs (Soltan 1982; see also Rees 1984). These simple and elegant arguments motivate the search for BHs in nearby galaxies (e.g., Kormendy & Richstone 1995; Magorrian et al. 1998; Gebhardt et al. 2003; Kormendy 2003). On the other hand, as a result of the endeavor in the past two decades, not only has the existence of the massive dark objects (which are presumably BHs here) in most nearby galactic centers been confirmed, but also dramatic progress on their demography has been recently achieved (e.g., Kormendy & Gebhardt 2001; Tremaine et al. 2002 and references therein). Comparisons between the properties of local BHs and those inferred from the QSO model may shed new light on our understanding of the BH growth, the accretion physics, the mechanisms to trigger and quench nuclear activities, the formation and evolution of galaxies etc. (e.g. Cavaliere & Padovani 1989; Small & Blandford 1992; Fabian & Iwasawa 1999; Salucci et al. 1999; Elvis, Risaliti & Zamorani 2002; Marconi & Salvati 2002; Yu & Tremaine 2002; Fabian 2003).

The comparison between the local BH mass density and the local energy density in QSO photons has suggested that local BHs acquire most of their mass through accretion during the QSO/AGN phase (Yu & Tremaine 2002; Aller & Richstone 2002; Fabian 2003). The mass distribution of local BHs as the remnant of nuclear activities is therefore controlled by the triggering history of the accretion onto seed BHs and the luminosity evolution of individual triggered nuclei with a mass-to-energy conversion efficiency  $\epsilon$  (i.e., the growth of individual BHs due to accretion). The triggering rate is usually believed to be related to the formation and evolution of galaxies and is a function of cosmic time, and the luminosity evolution of individual nuclei is believed to contain information on the accretion process in the vicinity of the BH and is a function of the physical time spent since the triggering of the accretion onto seed BHs. The triggering history and the luminosity evolution jointly control the QSO luminosity function (LF) as a function of luminosity and redshift; however, each cannot be uniquely determined from the QSOLF itself, partly as a result of the mixing of their effects on the QSOLF. In this paper, by using the local BH mass function (MF) as an additional constraint on QSO models and establishing a new relation between the QSOLF and the local BHMF, the luminosity evolution of individual QSOs is isolated from the triggering history of the QSO population in their effects on the QSOLF, and then we use observations to test QSO models and provide constraints on the QSO luminosity evolution and BH growth.

A relation between the QSOLF and the local BHMF has been achieved by Yu & Tremaine (2002) under the assumptions that the seed BH mass is negligible and the luminosities of QSOs are only an increasing function of their central BH mass. In the study of this paper, we relax these two assumptions. In addition, the relation in Yu & Tremaine (2002) includes the effect of BH mergers. However, BH mergers are ignored in the relation established in this paper for the following reasons: (i) BH mergers are not shown to play a significant role or not necessarily required at least for growth of high-mass ( $\gtrsim 10^8 M_\odot$ ) BHs, if  $\epsilon \simeq 0.1$  (Yu & Tremaine 2002); (ii) currently, the BH merger process and rate are very uncertain; and (iii) comparison of observations with the expectation obtained by ignoring BH mergers may also provide considerable insights in the role of BH mergers. The detailed difference between these two relations will be further discussed in this paper (see § 2.3 and 4.2.1).

This paper is organized as follows. In § 2, by studying the continuity equation for the BH mass and nuclear luminosity distribution, we establish the relation between the QSOLF and the local BHMF. The triggering history of the accretion onto seed BHs is (implicitly) considered in the continuity equation but circumvented in the relation between the QSOLF and local BHMF. Only the luminosity evolution of

individual QSOs is incorporated in this relation. In § 3 we obtain the local BHMF by using the Sloan Digital Sky Survey (SDSS) observation results on both early-type and late-type galaxies and the empirical relations on the demography of galaxies and BHs (the BH mass and velocity dispersion relation, the Tully-Fisher relation, etc.). We also review the QSOLF obtained from large optical surveys. In § 4 we combine the observations with the relation obtained in § 2 to provide accurate observational constraints on the luminosity evolution of individual QSOs and BH growth, such as the QSO lifetime, the mass-to-energy conversion efficiency, the role of obscuration in BH growth, etc. The results are discussed in § 5. In § 6 we further discuss some possible applications of the framework established in § 2, such as to the study of the demography of QSOs and the demography of normal galaxies at intermediate redshift. Finally, our conclusions are summarized in § 7.

In this paper we set the Hubble constant as  $H_0 = 100h \text{ km s}^{-1} \text{ Mpc}^{-1}$ , and if not otherwise specified, the cosmological model used is  $(\Omega_M, \Omega_\Lambda, h) = (0.3, 0.7, 0.65)$  (Wang et al. 2000).

## 2. The expected relation between the QSO luminosity function and the local BH mass function

### 2.1. The continuity equation

In this subsection we describe the evolution of the BH distribution by a continuity equation, which will be used to establish the relation between the QSOLF and the local BHMF.

We define  $\mathcal{N}(t_i, M_{\text{BH},0}, L, t)$  ( $t \geq t_i$ ) so that  $\mathcal{N}(t_i, M_{\text{BH},0}, L, t) dt_i dM_{\text{BH},0} dL dt$  is the comoving number density of local BHs with such properties: the nuclear activity due to accretion onto their seed BHs was triggered during cosmic time  $t_i \rightarrow t_i + dt_i$ , their nuclear luminosities were in the range  $L \rightarrow L + dL$  at cosmic time  $t$ , and these BHs have mass in the range  $M_{\text{BH},0} \rightarrow M_{\text{BH},0} + dM_{\text{BH},0}$  at present time  $t_0$ . We assume that the change rate of the nuclear luminosity  $\dot{L}$  is a function only of  $(t_i, M_{\text{BH},0}, L, t)$ . Ignoring BH mergers, we can use the following continuity equation to describe the evolution of  $\mathcal{N}(t_i, M_{\text{BH},0}, L, t)$ :

$$\frac{\partial \mathcal{N}(t_i, M_{\text{BH},0}, L, t)}{\partial t} + \frac{\partial [\dot{L}(t_i, M_{\text{BH},0}, L, t) \mathcal{N}(t_i, M_{\text{BH},0}, L, t)]}{\partial L} = 0. \quad (1)$$

We define the nuclear LF  $n_L(L, t)$  as follows:

$$n_L(L, t) \equiv \int_0^\infty dM_{\text{BH},0} \int_0^t dt_i \mathcal{N}(t_i, M_{\text{BH},0}, L, t) \quad (2)$$

so that  $n_L(L, t) dL$  is the number density of the local BHs that had nuclear luminosities in the range  $L \rightarrow L + dL$  at cosmic time  $t$ .

Below we illustrate the relation of equation (1) with some continuity equations of the QSOLF or BHMF in the literature (e.g., Caditz & Petrosian 1990; Small & Blandford 1992). By integrating equation (1) over  $M_{\text{BH},0}$  from 0 to  $\infty$  and over  $t_i$  from 0 to  $t$ , we may obtain the evolution of  $n_L(L, t)$  as follows:

$$\frac{\partial n_L(L, t)}{\partial t} + \frac{\partial [\langle \dot{L} \rangle n_L(L, t)]}{\partial L} = S(L, t), \quad (3)$$

where  $\langle \dot{L} \rangle(L, t)$  is the mean change rate of  $L$  defined by

$$\langle \dot{L} \rangle \equiv \frac{\int_0^\infty dM_{\text{BH},0} \int_0^t dt_i \dot{L}(t_i, M_{\text{BH},0}, L, t) \mathcal{N}(t_i, M_{\text{BH},0}, L, t)}{n_L(L, t)}, \quad (4)$$

and  $S(L, t)$  is the source function defined by

$$S(L, t) \equiv \int_0^\infty \mathcal{N}(t_i, M_{\text{BH},0}, L, t)|_{t_i=t} dM_{\text{BH},0} \quad (5)$$

and describing the triggering rate of nuclear activities of seed BHs. If  $\dot{L}(t_i, M_{\text{BH},0}, L, t)$  is a function only of  $L$  and  $t$  and  $n_L(L, t)$  is replaced by the QSOLF, equation (3) will be identical to equation (1) in Cavaliere et al. (1971) or equation (3) in Caditz & Petrosian (1990). If we replace  $L$  in equation (3) with BH mass of the progenitors of local BHs, equation (3) will look the same as equation (8) in Small & Blandford (1992) (which describes the evolution of the BHMF).

## 2.2. The time integrals of the nuclear/QSO luminosity function

By integrating equation (1) over  $L$  from 0 to  $\infty$ , we have the conservation of the number density

$$N(t_i, M_{\text{BH},0}, t) \equiv \int_0^\infty \mathcal{N}(t_i, M_{\text{BH},0}, L, t) dL \quad (6)$$

that is,

$$\frac{\partial N(t_i, M_{\text{BH},0}, t)}{\partial t} = 0. \quad (7)$$

According to equation (7), we have

$$N(t_i, M_{\text{BH},0}, t) = N(t_i, M_{\text{BH},0}, t_0), \quad (8)$$

For the same BH mass  $M_{\text{BH},0}$  at present, we assume that their nuclear luminosity evolution is a function only of the age of their nuclear activities  $\tau \equiv t - t_i$ . Thus, using equations (6) and (8), we have

$$\begin{aligned} \mathcal{N}(t_i, M_{\text{BH},0}, L, t) &= N(t_i, M_{\text{BH},0}, t) \delta[L - \mathcal{L}(M_{\text{BH},0}, \tau)] \\ &= N(t_i, M_{\text{BH},0}, t_0) \delta[L - \mathcal{L}(M_{\text{BH},0}, \tau)], \end{aligned} \quad (9)$$

where  $\delta(x)$  is the Dirac function and  $\mathcal{L}(M_{\text{BH},0}, \tau)$  is the nuclear luminosity of the progenitor of the BH  $M_{\text{BH},0}$  at age  $\tau$ . As seen from equations (2) and (9), the nuclear luminosity evolution (incorporated in the  $\delta$ -function) and the nuclear activity triggering history  $[N(t_i, M_{\text{BH},0}, t_0)]$  jointly contribute to the nuclear LF. By first integrating equation (9) over  $t_i$  from 0 to  $t$  and over  $t$  from 0 to  $t_0$  and then changing the integration variables  $(t, t_i)$  to  $(t_i, \tau)$ , we have

$$\begin{aligned} \int_0^{t_0} dt \int_0^t dt_i \mathcal{N}(t_i, M_{\text{BH},0}, L, t) &= \int_0^{t_0} dt \int_0^t dt_i N(t_i, M_{\text{BH},0}, t_0) \delta[L - \mathcal{L}(M_{\text{BH},0}, \tau)] \\ &= \int_0^{t_0} dt_i N(t_i, M_{\text{BH},0}, t_0) \int_0^{t_0-t_i} d\tau \delta[L - \mathcal{L}(M_{\text{BH},0}, \tau)] \\ &= \int_0^{t_0} dt_i N(t_i, M_{\text{BH},0}, t_0) \sum_k \frac{1}{|d\mathcal{L}(M_{\text{BH},0}, \tau)/d\tau|_{\tau=\tau_k}}, \end{aligned} \quad (10)$$

where  $\tau_k(L, M_{\text{BH},0})$  ( $k = 1, 2, \dots$ ) are the roots of the equation  $\mathcal{L}(M_{\text{BH},0}, \tau) - L = 0$  ( $0 < \tau < t_0 - t_i$ ).<sup>1</sup> We assume that the nuclear activities of all the local galaxies are quenched at present. Thus, for local BHs with

---

<sup>1</sup>In equation (10), it is assumed that  $d\mathcal{L}(M_{\text{BH},0}, \tau)/d\tau \neq 0$  at  $\tau = \tau_k$  ( $k = 1, 2, \dots$ ). Formulae (10), (11), (14) and (15) are not difficult to generalize even if  $d\mathcal{L}(M_{\text{BH},0}, \tau)/d\tau = 0$  at  $\tau = \tau_k$ , and other formulae will not be changed.

mass  $M_{\text{BH},0}$ , they have the same roots  $\tau_k(L, M_{\text{BH},0})$  ( $k = 1, 2, \dots$ ) for the same  $L$  since they have experienced the same evolution of  $\mathcal{L}(M_{\text{BH},0}, \tau)$  before their quenching, even though their accretion onto their seed BHs may be triggered at different time  $t_i$ . Hence, the sum term  $\sum_k$  in equation (10) does not depend on  $t_i$ , and we have

$$\int_0^{t_0} dt \int_0^t dt_i \mathcal{N}(t_i, M_{\text{BH},0}, L, t) = n_{\text{MBH}}(M_{\text{BH},0}, t_0) \sum_k \frac{1}{|\text{d}\mathcal{L}(M_{\text{BH},0}, \tau)/\text{d}\tau|_{\tau=\tau_k}}, \quad (11)$$

where

$$n_{\text{MBH}}(M_{\text{BH},0}, t_0) \equiv \int_0^{t_0} N(t_i, M_{\text{BH},0}, t_0) dt_i \quad (12)$$

is the local BHMF and  $n_{\text{MBH}}(M_{\text{BH},0}, t_0) \text{d}M_{\text{BH},0}$  gives the number density of local BHs with mass in the range  $M_{\text{BH},0} \rightarrow M_{\text{BH},0} + \text{d}M_{\text{BH},0}$ . The lifetime of the nuclear activity for the BH with current mass  $M_{\text{BH},0}$  can be expressed by

$$\tau_{\text{life}}(M_{\text{BH},0}) = \int \text{d}\tau \quad (13)$$

$$= \int \text{d}L \sum_k \frac{1}{|\text{d}\mathcal{L}(M_{\text{BH},0}, \tau)/\text{d}\tau|_{\tau=\tau_k}}. \quad (14)$$

Note that the integration in equation (13) is over the period when the nucleus is active, and equation (14) is also restricted to the luminosity  $\mathcal{L}(M_{\text{BH},0}, \tau)$  that is taken as active (e.g., higher than a certain luminosity limit). The definition of “active” of galactic nuclei may be different in different contexts, and equations (13) and (14) (such as their integration limits) may be adjusted to appropriate forms according to different definitions. During the period of the nuclear activity, the fraction of the time (or the probability) with luminosity in the range  $L \rightarrow L + \text{d}L$  can be given by

$$P(L|M_{\text{BH},0})\text{d}L \equiv \frac{\text{d}L}{\tau_{\text{life}}(M_{\text{BH},0})} \sum_k \frac{1}{|\text{d}\mathcal{L}(M_{\text{BH},0}, \tau)/\text{d}\tau|_{\tau=\tau_k}} \quad (15)$$

with

$$\int P(L|M_{\text{BH},0})\text{d}L = 1. \quad (16)$$

Applying equations (14) and (15) in equation (11), we have

$$\int_0^{t_0} dt \int_0^t dt_i \mathcal{N}(t_i, M_{\text{BH},0}, L, t) = n_{\text{MBH}}(M_{\text{BH},0}, t_0) \tau_{\text{life}}(M_{\text{BH},0}) P(L|M_{\text{BH},0}). \quad (17)$$

By integrating equation (17) over  $M_{\text{BH},0}$  and using equation (2), we have the time integral of the nuclear LF as follows:

$$\int_0^{t_0} n_L(L, t) dt = \int_0^\infty \text{d}M_{\text{BH},0} n_{\text{MBH}}(M_{\text{BH},0}, t_0) \tau_{\text{life}}(M_{\text{BH},0}) P(L|M_{\text{BH},0}) \equiv \mathcal{T}_{L,\text{local}}(L, t_0). \quad (18)$$

We define the QSOLF  $\Psi_L(L, t)$  so that  $\Psi_L(L, t)\text{d}L$  is the comoving number density of QSOs with luminosity in the range  $L \rightarrow L + \text{d}L$  at cosmic time  $t$ , and we define the time integral of the QSOLF as follows:

$$\mathcal{T}_{L,\text{QSO}}(L, t_0) \equiv \int_0^{t_0} \Psi_L(L, t) dt. \quad (19)$$

The QSOLF in equation (19) includes the contribution from both optically bright QSOs and any other QSOs that are obscured or not seen in optical bands but might be detectable in other bands (see Fabian 2003). In this paper  $\Psi_L(L, t)$  denotes the LF of the “live” QSOs in the distant universe and  $n_L(L, t)$  denotes the nuclear LF of the progenitors of the local BHs. Based on the cosmological principle, similar to Soltan’s argument (1982), the QSOLF  $\Psi_L(L, t)$  represents the evolution of the nuclear luminosity of local BHs, i.e.,

$$n_L(L, t) = \Psi_L(L, t). \quad (20)$$

Thus, with equations (18)–(20), we have

$$\mathcal{T}_{L, \text{QSO}}(L, t_0) = \mathcal{T}_{L, \text{local}}(L, t_0). \quad (21)$$

The physical meaning of equations (18) and (21) can be understood clearly as follows. For the progenitor of each local BH with mass  $M_{\text{BH},0}$ , the average time that it has spent in the nuclear luminosity range  $L \rightarrow L + dL$  is  $\tau_{\text{life}}(M_{\text{BH},0})P(L|M_{\text{BH},0})$ , and taking QSOs as the progenitors of the local BHs, the total time spent in the range  $L \rightarrow L + dL$  by the progenitors of all the local BHs with mass  $M_{\text{BH},0}$  in a unit comoving volume should just be the time integral of  $\Psi_L(L, t)dL$ . We note that the quantity of the time integral of the QSOLF has been (implicitly) used before in the literature, such as in some BH mass density relations between local BHs and QSOs or the definition of the QSO mean lifetime, which will be further discussed in § 2.3, and we also note that Blandford (2003) points out that a simple model of accretion implies a quantitative relationship between the time integral of the QSOLF and the local BHMF. Relation (21) established above on the time integral of the QSOLF will be the base to constrain the luminosity evolution of QSOs and BH growth in this paper.

In addition, note that in equation (21) or (18) the luminosity  $L$  is assumed to be only a function of  $M_{\text{BH},0}$  and  $\tau$ . For the more complicated case that  $L$  also depends on some other parameters, we may take the lifetime and probability function in equation (18) as the averaged result over other parameters or generalize these equations by including other parameters.

### 2.3. Mean lifetime, and total/partial BH mass densities

Below we show with appropriate assumptions, how the definition of the mean QSO lifetime and some relations on the BH mass density obtained in the literature (e.g., Soltan 1982; Yu & Tremaine 2002; Haiman, Ciotti & Ostriker 2003) can be incorporated in the framework established above:

- Mean QSO lifetime: the lifetime  $\tau_{\text{life}}(M_{\text{BH},0})$  in equation (18) also represents the lifetime of “live” QSOs whose central BH masses will be  $M_{\text{BH},0}$  at present. By integrating equation (21) over  $L$  and using equation (16), we have

$$\int dL \int_0^{t_0} \Psi_L(L, t) dt = \int_0^\infty dM_{\text{BH},0} n_{M_{\text{BH}}}(M_{\text{BH},0}, t_0) \tau_{\text{life}}(M_{\text{BH},0}). \quad (22)$$

We may define the mean lifetime of QSOs as follows:

$$\langle \tau_{\text{life}} \rangle \equiv \frac{\int_0^\infty dM_{\text{BH},0} n_{M_{\text{BH}}}(M_{\text{BH},0}, t_0) \tau_{\text{life}}(M_{\text{BH},0})}{\int_0^\infty dM_{\text{BH},0} n_{M_{\text{BH}}}(M_{\text{BH},0}, t_0) H[\tau_{\text{life}}(M_{\text{BH},0})]} = \frac{\int dL \int_0^{t_0} \Psi_L(L, t) dt}{\int_0^\infty dM_{\text{BH},0} n_{M_{\text{BH}}}(M_{\text{BH},0}, t_0) H[\tau_{\text{life}}(M_{\text{BH},0})]}, \quad (23)$$

where equation (22) is used and  $H(x)$  is the Heaviside step function defined by  $H(x) = 1$  if  $x > 0$  and  $H(x) = 0$  otherwise. We denote the mass of the progenitors of the local BHs when they had a nuclear

luminosity  $L$  (or the central BH mass of a QSO with luminosity  $L$ ) as  $M_{\text{BH}}$ . If  $L$  is an increasing function only of  $M_{\text{BH}}$  and only the period with luminosities brighter than a certain value  $L(M'_{\text{BH}})$  is taken as active phase, we have  $\tau_{\text{life}}(M_{\text{BH},0}) > 0$  if  $M_{\text{BH},0} > M'_{\text{BH}}$  and  $\tau_{\text{life}}(M_{\text{BH},0}) = 0$  otherwise. Thus, the mean lifetime of QSOs is given by

$$\langle \tau_{\text{life}} \rangle = \frac{\int_{L(M'_{\text{BH}})}^{\infty} dL \int_0^{t_0} \Psi_L(L, t) dt}{\int_{M'_{\text{BH}}}^{\infty} n_{M_{\text{BH}}}(M_{\text{BH},0}, t_0) dM_{\text{BH},0}}, \quad (24)$$

which is identical to equation (59) in Yu & Tremaine (2002; see also eq. [24] in Haiman, Ciotti & Ostriker 2003).

- Total BH mass densities: we denote the QSO bolometric luminosity produced by a mass accretion rate  $\dot{M}_{\text{acc}}$  as  $L_{\text{bol}} = \epsilon \dot{M}_{\text{acc}} c^2 = \epsilon \dot{M}_{\text{BH}} / (1 - \epsilon)$ , where  $\dot{M}_{\text{BH}} = \dot{M}_{\text{acc}} (1 - \epsilon)$  is the growth rate of BH mass and  $c$  is the speed of light. (The subscript “bol” represents the bolometric luminosity, and the symbol  $L$  in this paper may be either the bolometric luminosity or the luminosity in a specific band, if not specified.) By multiplying equation (21) by  $(1 - \epsilon)L_{\text{bol}}/(\epsilon c^2) = \dot{M}_{\text{BH}}$  and then integrating over  $L$  from a given value  $L'$  to  $\infty$ , we have

$$\int_{L'}^{\infty} dL \frac{(1 - \epsilon)L_{\text{bol}}}{\epsilon c^2} \int_0^{t_0} \Psi_L(L, t) dt = \int_0^{\infty} dM_{\text{BH},0} n_{M_{\text{BH}}}(M_{\text{BH},0}, t_0) \int_{L'}^{\infty} dL \dot{M}_{\text{BH}} \tau_{\text{life}}(M_{\text{BH},0}) P(L|M_{\text{BH},0}). \quad (25)$$

By setting  $L' = 0$ , equation (25) becomes

$$\int_0^{\infty} dL \frac{(1 - \epsilon)L_{\text{bol}}}{\epsilon c^2} \int_0^{t_0} \Psi_L(L, t) dt = \int_0^{\infty} dM_{\text{BH},0} M_{\text{BH},0} n_{M_{\text{BH}}}(M_{\text{BH},0}, t_0), \quad (26)$$

where

$$\int_0^{\infty} dL \dot{M}_{\text{BH}} \tau_{\text{life}}(M_{\text{BH},0}) P(L|M_{\text{BH},0}) = \int_0^{t_0} \dot{M}_{\text{BH}} dt = M_{\text{BH},0} - \langle M_{\text{BH},i} \rangle (M_{\text{BH},0}) \quad (27)$$

is used;  $\langle M_{\text{BH},i} \rangle (M_{\text{BH},0})$  is the average mass of the seed BHs that will have mass  $M_{\text{BH},0}$  at present and is ignored in equation (26). Equation (26) is identical to Sołtan’s argument (1982) relating the total local energy density in QSOs to the total BH mass density in nearby galaxies.

- Partial BH mass densities: if the QSO luminosity  $L$  is only an increasing function of the BH mass  $M_{\text{BH}}$ , we have

$$\begin{aligned} & \int_{L'}^{\infty} dL \dot{M}_{\text{BH}} \tau_{\text{life}}(M_{\text{BH},0}) P(L|M_{\text{BH},0}) \\ &= \begin{cases} M_{\text{BH},0} - \max[M_{\text{BH}}(L'), M_{\text{BH},i}(M_{\text{BH},0})], & \text{if } M_{\text{BH},0} > \max[M_{\text{BH}}(L'), M_{\text{BH},i}(M_{\text{BH},0})] \\ 0, & \text{otherwise} \end{cases} \end{aligned} \quad (28)$$

where the seed BH mass  $M_{\text{BH},i}$  is assumed to be a function only of  $M_{\text{BH},0}$ . By applying equation (28) in equation (25) and assuming  $M_{\text{BH},i}(M_{\text{BH},0}) < M_{\text{BH}}(L')$ , we have

$$\int_{L'}^{\infty} dL \frac{(1 - \epsilon)L_{\text{bol}}}{\epsilon c^2} \int_0^{t_0} \Psi_L(L, t) dt = \int_{M_{\text{BH}}(L')}^{\infty} dM_{\text{BH},0} [M_{\text{BH},0} - M_{\text{BH}}(L')] n_{M_{\text{BH}}}(M_{\text{BH},0}, t_0). \quad (29)$$

Actually, even if the seed BH mass is not a function only of  $M_{\text{BH},0}$ , equation (29) will still hold at a given  $L'$  as long as all the seed BH masses of the local BHs  $M_{\text{BH},0} [ > M_{\text{BH}}(L') ]$  are smaller than  $M_{\text{BH}}(L')$ . Equation (29) is identical to the relation between the partial BH mass density in nearby galaxies and that accreted during bright QSO phases in Yu & Tremaine (2002) if BH mergers are ignored (see eq. 30 in Yu & Tremaine 2002).

## 2.4. $\mathcal{L}(M_{\text{BH},0}, \tau)$

Given the QSOLF and local BHMF, the nuclear luminosity evolution [or  $\tau_{\text{life}}(M_{\text{BH},0})P(L|M_{\text{BH},0})$ ] cannot be uniquely determined from equations (18)–(21). Below we use some physical arguments to assume a form of the luminosity evolution  $\mathcal{L}(M_{\text{BH},0}, \tau)$ . The parameters involved in the assumed form will be constrained by observations in § 4.2.

It is generally believed that the growth of a BH involves two phases after the nuclear activity is triggered on (see the discussion on the “feast and famine” model in Small & Blandford 1992 and Blandford 2003). In the first (or “demand limited”) phase, there is plenty of material to supply for the BH growth; however, not all of the available material can contribute to the BH growth at once and the BH growth is limited by the Eddington luminosity. With the decline of material supply, the BH growth enters into the second (or “supply limited”) phase and the nuclear luminosity is expected to decline below the Eddington luminosity. For simplicity, we assume that the two phases appear only once in this paper, although this assumption is not required in relation (21). The possibility of more complicated accretion patterns deserves further investigation by applying corresponding models in relation (21).

In the first phase, after the BH is triggered at time  $t_i$ , we assume that it accretes with the Eddington luminosity for a time  $\tau_1$  and its mass increases to be  $M_{\text{BH},\text{I}}$  at time  $t = t_i + \tau_1 \equiv t_1$ . The mass-to-energy conversion efficiency  $\epsilon$  is assumed to be a constant. Thus, the nuclear luminosity in the first phase increases with time as follows:

$$\mathcal{L}_{\text{bol}}(\tau) = L_{\text{Edd}}(M_{\text{BH},\text{I}}) \exp\left(\frac{\tau - \tau_1}{\tau_{\text{Sp}}}\right), \quad 0 < \tau < \tau_1, \quad (30)$$

where  $L_{\text{Edd}}(M_{\text{BH}})$  is the Eddington luminosity of a BH with mass  $M_{\text{BH}}$  and

$$\tau_{\text{Sp}} = 4.5 \times 10^7 \left[ \frac{\epsilon}{0.1(1 - \epsilon)} \right] \text{ yr} \quad (31)$$

is the Salpeter time (the time for a BH radiating at the Eddington luminosity to e-fold in mass). In the second phase, we assume that the evolution of the nuclear luminosity declines as follows (e.g., Haehnelt, Natarajan & Rees 1998; Haiman & Loeb 1998):

$$\mathcal{L}_{\text{bol}}(\tau) = \begin{cases} L_{\text{Edd}}(M_{\text{BH},\text{I}}) \exp\left(-\frac{\tau - \tau_1}{\tau_{\text{D}}}\right), & \text{for } \tau_1 \leq \tau \leq \tau_1 + \xi\tau_{\text{D}}, \\ 0, & \text{for } \tau > \tau_1 + \xi\tau_{\text{D}}, \end{cases} \quad (32)$$

where  $\tau_{\text{D}}$  is the characteristic declining timescale of the nuclear luminosity. We assume that QSOs become quiescent when the nuclear luminosity declines by a factor of  $\eta = \exp(-\xi)$  compared to the peak luminosity  $L_{\text{Edd}}(M_{\text{BH},\text{I}})$ , so there is a cutoff of the nuclear luminosity at  $\tau = \tau_1 + \xi\tau_{\text{D}}$  in equation (32). The factor  $\xi$  is set to  $-\ln(10^{-3}) = 6.9$  here, since after decreasing by a factor of  $\eta = 10^{-3}$ , the nuclear luminosity of BHs even with a high mass  $\sim 10^9 M_{\odot}$  will become fainter than the luminosity range ( $M_B \lesssim -20$  in § 4) of interest in this paper. With the assumption that all QSOs are quenched at present (i.e.,  $t_0 - t_i - \tau_1 \gg \tau_{\text{D}}$ ), the BH mass at present is given by

$$M_{\text{BH},0} = M_{\text{BH},\text{I}} + \int_{t_i}^{t_0} \frac{(1 - \epsilon)L_{\text{bol}}}{\epsilon c^2} dt = \left(1 + \frac{\tau_{\text{D}}}{\tau_{\text{Sp}}}\right) M_{\text{BH},\text{I}}. \quad (33)$$

In equation (33), the efficiency  $\epsilon$  is assumed to be the same as the efficiency in the first phase and not to change with the decline of the nuclear luminosity. It is important to know how the realistic efficiency evolves with the change of the nuclear luminosity or other parameters (which would depend on the evolution of both



the accretion rates and BH spins; a detailed study about this is beyond the scope of this paper). If the nuclear luminosity of a BH is smaller than its Eddington luminosity by a factor of 10 or more, according to current accretion models, the BH might accrete material via the advection-dominated accretion flow (ADAF) with low efficiency  $\epsilon \ll 0.1$  (e.g., Narayan & Yi 1994), rather than via the thin-disk accretion with efficiency  $\epsilon \sim 0.1 - 0.3$  near the Eddington luminosity. Considering this possibility of the very low efficiency at the late stage of the luminosity evolution, the contribution from the very low efficiency stage to the time integral of the nuclear LF (in the luminosity range  $M_B < -20$  shown in this paper) is insignificant and our conclusions will still hold for other stages of the nuclear activity (which can be inferred from the results obtained in § 4.2). We also assume that  $\epsilon$  is irrelevant to the BH mass  $M_{\text{BH},0}$  in this paper.

By using equations (30)–(33) in equations (14) and (15), we have the QSO lifetime given by

$$\tau_{\text{life}} = \tau_{\text{I}} + \xi \tau_{\text{D}}, \quad (34)$$

and the BH with present mass  $M_{\text{BH},0}$  has such a probability distribution of the nuclear bolometric luminosity in its evolution history:

$$P(L_{\text{bol}}|M_{\text{BH},0}) = \frac{1}{\tau_{\text{life}}} \left( f_{\text{I}} \frac{\tau_{\text{Sp}}}{L_{\text{bol}}} + f_{\text{D}} \frac{\tau_{\text{D}}}{L_{\text{bol}}} \right), \quad (35)$$

where

$$f_{\text{I}} = \begin{cases} 1, & \text{if } L_{\text{Edd}}(M_{\text{BH},\text{I}}) \exp(-\tau_{\text{I}}/\tau_{\text{Sp}}) \leq L_{\text{bol}} \leq L_{\text{Edd}}(M_{\text{BH},\text{I}}) \\ 0, & \text{otherwise} \end{cases}, \quad (36)$$

and

$$f_{\text{D}} = \begin{cases} 1, & \text{if } L_{\text{Edd}}(M_{\text{BH},\text{I}}) \exp(-\xi) \leq L_{\text{bol}} \leq L_{\text{Edd}}(M_{\text{BH},\text{I}}) \\ 0, & \text{otherwise} \end{cases}. \quad (37)$$

In the analysis above, the timescales  $\tau_{\text{I}}$  and  $\tau_{\text{D}}$  are not necessarily constants, and they may be a function of  $M_{\text{BH},0}$ . The dependence of  $\tau_{\text{I}}$  on  $M_{\text{BH},0}$  would depend on the distribution of seed BHs, which are poorly known and beyond the scope of this paper. Below we always assume that  $\tau_{\text{I}}$  and  $\tau_{\text{D}}$  are irrelevant to  $M_{\text{BH},0}$ .

### 3. The local BH mass function and QSO luminosity function obtained from observations

#### 3.1. The local BH mass function $n_{\text{MBH}}(M_{\text{BH},0}, t_0)$

In this subsection we use the velocity-dispersion distribution of local galaxies (§ 3.1.1) and the empirical BH mass-velocity dispersion relation (§ 3.1.2) to obtain the local BHMF (§ 3.1.3).

##### 3.1.1. Local velocity-dispersion function $n_{\sigma}(\sigma, t_0)$

We define  $n_{\sigma}(\sigma, t_0)$  as the velocity-dispersion function of the hot stellar components of local galaxies so that  $n_{\sigma}(\sigma, t_0)d\sigma$  represents the comoving number density of local galaxies in the range  $\sigma \rightarrow \sigma + d\sigma$  (by “hot” component we mean either an elliptical galaxy or the bulge of a spiral or S0 galaxy). The velocity-dispersion distribution  $n_{\sigma}(\sigma, t_0)$  includes the contribution by both early-type galaxies  $n_{\sigma}^{\text{early}}(\sigma, t_0)$  and late-type galaxies  $n_{\sigma}^{\text{late}}(\sigma, t_0)$ , that is,

$$n_{\sigma}(\sigma, t_0) = n_{\sigma}^{\text{early}}(\sigma, t_0) + n_{\sigma}^{\text{late}}(\sigma, t_0). \quad (38)$$

Recent study on a sample of nearly 9000 nearby early-type galaxies obtained by the SDSS has provided the velocity-dispersion distribution in early-type galaxies as follows (see eq. 4 in Sheth et al. 2003, and Bernardi et al. 2003):

$$n_{\sigma}^{\text{early}}(\sigma, t_0) = \phi_* \left( \frac{\sigma}{\sigma_*} \right)^{\alpha} \frac{\exp [-(\sigma/\sigma_*)^{\beta}]}{\Gamma(\alpha/\beta)} \frac{\beta}{\sigma}, \quad (39)$$

where the best-fit values of  $(\phi_*, \sigma_*, \alpha, \beta)$  are  $(0.0016 \pm 0.0001, 88.8 \pm 17.7, 6.5 \pm 1.0, 1.93 \pm 0.22)$ ,  $\phi_*$  is the comoving number density of local early-type galaxies in units of  $\text{Mpc}^{-3}$ , and  $\sigma_*$  is in units of  $\text{km s}^{-1}$ .

We obtain the velocity-dispersion distribution in local late-type galaxies  $n_{\sigma}^{\text{late}}(\sigma, t_0)$  in the following steps: (i) Following Sheth et al. (2003), we get the LF of the late-type galaxies by subtracting the LF of the early-type galaxies (Blanton et al. 2003) from the LF of total galaxies (Bernardi et al. 2003). (ii) Following Sheth et al. (2003), we get the distribution of the circular velocity  $v_c$  in late-type galaxies by using the LF of the late-type galaxies obtained above and the following Tully-Fisher relation (Giovanelli et al. 1997):

$$\log(2v_c) = 1.10 - (M_I - 5 \log h)/7.95, \quad (40)$$

where  $M_I$  is the absolute magnitude of the galaxies in the  $I$  band, accounting for the intrinsic scatters around relation (40) and the inclination effects of galaxies (see details in Sheth et al. 2003). (iii) We get the velocity-dispersion function of late-type galaxies by using the circular-velocity distribution of the late-type galaxies obtained above and the following correlation between the circular velocity and the velocity dispersion of the bulge component (see eq. 3 in Baes et al. 2003; see also Ferrarese 2002):

$$\log \left( \frac{v_c}{200 \text{ km s}^{-1}} \right) = (0.96 \pm 0.11) \log \left( \frac{\sigma}{200 \text{ km s}^{-1}} \right) + (0.21 \pm 0.023). \quad (41)$$

The intrinsic scatter of the correlation given by (41) is small ( $< 0.15$  dex; see Fig. 1 in Baes et al. 2003) and ignored in our calculation. Relation (41) may not hold for  $\sigma < 80 \text{ km s}^{-1}$ , which corresponds to BH mass  $\lesssim 4 \times 10^6 M_{\odot}$  according to the BH mass-velocity dispersion relation below (eq. 42) and is beyond the range that we focus on in § 4.2.

### 3.1.2. The BH mass and velocity dispersion relation

Studies of central BHs in nearby galaxies have revealed that the BH mass and the velocity dispersion of the hot stellar component of the host galaxy follow a tight correlation (Tremaine et al. 2002; Ferrarese & Merritt 2000; Gebhardt et al. 2000). The logarithmic of the BH mass at a given velocity dispersion  $\sigma$  has a mean value given by (Tremaine et al. 2002)

$$\langle \log(M_{\text{BH},0}) | \sigma_e \rangle = A + \gamma \log(\sigma_e/200 \text{ km s}^{-1}), \quad (42)$$

where  $M_{\text{BH},0}$  is in units of  $M_{\odot}$ ,  $\gamma = 4.02 \pm 0.32$ ,  $A = 8.18 \pm 0.06$  have been adjusted to our assumed Hubble constant  $h = 0.65$  (see section 2.2 in Yu & Tremaine 2002), and  $\sigma_e$  is the luminosity-weighted line-of-sight velocity dispersion within a slit extending to the effective radius. Note that  $\sigma_e$  in the correlation (42) is the velocity dispersion within a slit extending to the effective radius  $R_o$  (Gebhardt et al. 2000), while  $\sigma$  in the SDSS (eq. 39) is the velocity dispersion within a circular aperture extending to  $R_o/8$ . However, replacing  $\sigma_e$  with  $\sigma$  in equation (42) will not cause much difference as the two definitions should give very similar results (Tremaine et al. 2002). Merritt & Ferrarese (2001) give an alternative version of the correlation (42) with a steeper slope,  $\gamma = 4.72$ . The reasons for this difference in slopes are discussed by Tremaine et al. (2002). We

perform the calculations using both versions of the correlation and the difference on the local BHMF will be discussed in § 3.1.3.

Note that relation (42) is fitted in the  $\log M_{\text{BH},0}$ – $\log \sigma$  space. We assume that the distribution in  $\log M_{\text{BH},0}$  at a given  $\sigma$  is Gaussian with intrinsic standard deviation  $\Delta_{\log M_{\text{BH},0}}$ , which is independent of  $\sigma$  and thus can be written as

$$P(\log M_{\text{BH},0}|\sigma) = \frac{1}{\sqrt{2\pi}\Delta_{\log M_{\text{BH},0}}} \exp \left[ -\frac{(\log M_{\text{BH},0} - \langle \log M_{\text{BH},0}|\sigma \rangle)^2}{2\Delta_{\log M_{\text{BH},0}}^2} \right]. \quad (43)$$

According to Tremaine et al. (2002), the intrinsic scatter in  $\log M_{\text{BH},0}$  should not be larger than 0.25–0.3 dex. Nevertheless, to check the effect of  $\Delta_{\log M_{\text{BH},0}}$  on the results, below we show the results obtained with a value of  $\Delta_{\log M_{\text{BH},0}}$  (= 0.4 dex) higher than 0.27 dex, as well as those obtained with  $\Delta_{\log M_{\text{BH},0}} = 0$  and 0.27 dex.

With the velocity-dispersion function and the BH mass–velocity dispersion relation (eqs. 42 and 43), the local BHMF is given by

$$n_{\text{MBH}}(M_{\text{BH},0}, t_0) = \ln 10 \int M_{\text{BH},0} P(\log M_{\text{BH},0}|\sigma) n_{\sigma}(\sigma, t_0) d\sigma. \quad (44)$$

### 3.1.3. Results: $n_{\text{MBH}}(M_{\text{BH},0}, t_0)$

Using the velocity-dispersion function in § 3.1.1, the BH mass–velocity dispersion relation in § 3.1.2, and equation (44), we obtain the local BHMF  $n_{\text{MBH}}(M_{\text{BH},0}, t_0)$  and show the distribution of  $M_{\text{BH},0} n_{\text{MBH}}(M_{\text{BH},0}, t_0)$  in Figure 1. In Figure 1a, different solid lines represent the results obtained with different  $\Delta_{\log M_{\text{BH},0}}$  (=0, 0.27, and 0.4 dex from bottom to top at the high-mass end, respectively, see eq. 43). As seen from panel (a), the local BHMF at the high-mass end ( $\gtrsim 3 \times 10^8 M_{\odot}$ ) is significantly affected by the intrinsic scatter  $\Delta_{\log M_{\text{BH},0}}$ . For example, the BHMF obtained with  $\Delta_{\log M_{\text{BH},0}} = 0.27$  dex (middle solid line) is larger than that obtained with  $\Delta_{\log M_{\text{BH},0}} = 0$  (bottom solid line) by a factor of 5 at  $M_{\text{BH},0} \simeq 10^9 M_{\odot}$  and by a factor of more than 10 at  $M_{\text{BH},0} \simeq 4 \times 10^9 M_{\odot}$  and if  $\Delta_{\log M_{\text{BH},0}} = 0.4$  dex, the BHMF (top solid line) is larger than that obtained with  $\Delta_{\log M_{\text{BH},0}} = 0$  by a factor of 8 at  $M_{\text{BH},0} \simeq 10^9 M_{\odot}$  and a factor of more than 100 at  $M_{\text{BH},0} \simeq 4 \times 10^9 M_{\odot}$ . The solid lines are the results obtained by setting the variables  $(\phi_*, \sigma_*, \alpha, \beta)$  in equation (39) to the mean of the best-fit values. We also show the uncertainty of the local BHMF due to the 1- $\sigma$  error of the fitting values in the velocity-dispersion function of early-type galaxies in panel (a). The two dotted lines adjacent to each solid line represent the result after considering the 1- $\sigma$  error of the mean value of  $(\sigma_*, \alpha, \beta)$  in equation (39), which is obtained by setting  $(\sigma_*, \alpha, \beta) = (88.8, 6.5, 1.93) \pm (+17.7, -1.0, +0.22)$ . Note that the signs set to the errors of the variables are not all the same because the best-fit values of  $(\sigma_*, \alpha, \beta)$  are strongly correlated with one another (see fig. 4 in Sheth et al. 2003). We do not consider the error in  $\phi_*$  here since it is small and the uncertainty caused by it is negligible compared to that caused by the error of other variables. As seen from panel (a), the uncertainty of the local BHMF due to the uncertainty in the velocity-dispersion function of early-type galaxies is negligible compared to that due to the intrinsic scatter  $\Delta_{\log M_{\text{BH},0}}$  in the  $M_{\text{BH},0} - \sigma$  relation. In panel (a), the dashed lines show the local BHMF in late-type galaxies also obtained with  $\Delta_{\log M_{\text{BH},0}} = 0, 0.27$  and 0.4 dex from bottom to top at the high-mass end, respectively. So far, it is hard to give an accurate estimate of the uncertainty in the estimate of the velocity-dispersion function of late-type galaxies here. We believe that the effect on the local BHMF due to the uncertainty in the velocity-dispersion function of the late-type galaxies can be ignored at the high-mass end ( $\gtrsim 4 \times 10^7 M_{\odot}$ ), where the local BHMF is dominated by early-type galaxies. The local BHMF

is dominated by late-type galaxies at the low-mass end ( $\lesssim 10^7 M_\odot$ ). We expect that the local BHMF with BH mass in the range from  $4 \times 10^6 M_\odot$  to  $4 \times 10^7 M_\odot$  has considerable accuracy, for example, within 50%.

In Figure 1b we show the effect on the local BHMF due to different versions of the slope  $\gamma$  in the  $M_{\text{BH},0} - \sigma$  relation (eq. 42). The solid lines are the same as those in panel (a), which are obtained with  $\gamma = 4.02$  (Tremaine et al. 2002). The dot-dashed lines are obtained with  $\gamma = 4.72$  (Merritt & Ferrarese 2001). As seen from panel (b), the difference of the BHMF at the high-mass end due to the difference in  $\gamma$  is not so significant as that due to the difference of the intrinsic scatter  $\Delta_{\log M_{\text{BH},0}}$  in the  $M_{\text{BH},0} - \sigma$  relation. Below we always show the results obtained with  $\gamma = 4.02$  (Tremaine et al. 2002).

In principal, the local BHMF can also be obtained by using the luminosity distribution of the hot stellar components of local galaxies and its correlation with central BHs (e.g., Kormendy & Gebhardt 2001). However, we do not do so in this paper, because the total local BH mass density obtained by using the BH mass – luminosity relation appears to be larger than that obtained by using the BH mass – velocity dispersion relation by a factor of more than 2, and the reason for this difference is not yet clear (Yu & Tremaine 2002). As argued in Yu & Tremaine (2002), we believe that the results obtained by using the BH mass – velocity dispersion relation are more reliable, as the correlation between the BH mass and the velocity dispersion is tighter and the result does not depend on the uncertain bulge-disk decomposition.

Note that although the local BHMF at the high-mass end is significantly affected by the intrinsic scatter in the  $M_{\text{BH},0} - \sigma$  relation, the total local BH mass density is not, which is higher than the total density obtained by setting  $\Delta_{\log M_{\text{BH},0}} = 0$  only by a factor of  $\exp[\frac{1}{2}(\Delta_{\log M_{\text{BH},0}} \ln 10)^2]$  (=1.2 if  $\Delta_{\log M_{\text{BH},0}} = 0.27$  dex and 1.5 if  $\Delta_{\log M_{\text{BH},0}} = 0.4$  dex (see eq. 12 in Yu & Tremaine 2002)).

### 3.2. The luminosity function of optically bright QSOs

The LF of optically bright QSOs is often fitted with a double power law:

$$\Psi_{M_B}^{\text{opt}}(M_B, z) = \frac{\Psi_M^*}{10^{0.4(\beta_1+1)[M_B-M_B^*(z)]} + 10^{0.4(\beta_2+1)[M_B-M_B^*(z)]}}, \quad (45)$$

where the superscript “opt” represents optically bright (or unobscured) QSOs,  $\Psi_{M_B}^{\text{opt}}(M_B, z)dM_B$  is the comoving number density of QSOs with absolute magnitude in the range  $[M_B, M_B + dM_B]$  at redshift  $z$ , and we have

$$\Psi_{M_B}(M_B, z) = \Psi_{L_B}(L_B, z)|dL_B/dM_B| = 0.92L_B\Psi(L_B, z). \quad (46)$$

Pei (1995) uses this form to fit the data set from Hartwick & Schade (1990) and Warren, Hewett, & Osmer (1995) on the basis of more than 1200 QSOs over the range of redshift  $0.1 < z < 4.5$ . In the cosmological model of  $(\Omega_m, \Omega_\Lambda, h) = (1, 0, 0.5)$ , the QSOLF with absolute magnitudes  $-30 \lesssim M_B \lesssim -23$  can be fitted by equation (45) with the following parameters:

$$\Psi_M^* = 6.7 \times 10^{-6} h^3 \text{Mpc}^{-3} \text{mag}^{-1}, \quad (47)$$

$$M_B^*(z) = M_B^*(0) + 1.25 \log(1+z) - 2.5(k_1 z + k_2 z^2), \quad (48)$$

$$M_B^*(0) = -20.83 + 5 \log h, k_1 = 1.39, k_2 = -0.25, \quad (49)$$

$$\beta_1 = -1.64 \text{ and } \beta_2 = -3.52. \quad (50)$$

Note that the cosmological model in which the parameters above are fitted is different from the model adopted in this paper. In our calculations below, we have transferred the parameters in equations (47)–(50) into the cosmological model used in this paper,  $(\Omega_m, \Omega_\Lambda, h) = (0.3, 0.7, 0.65)$ .

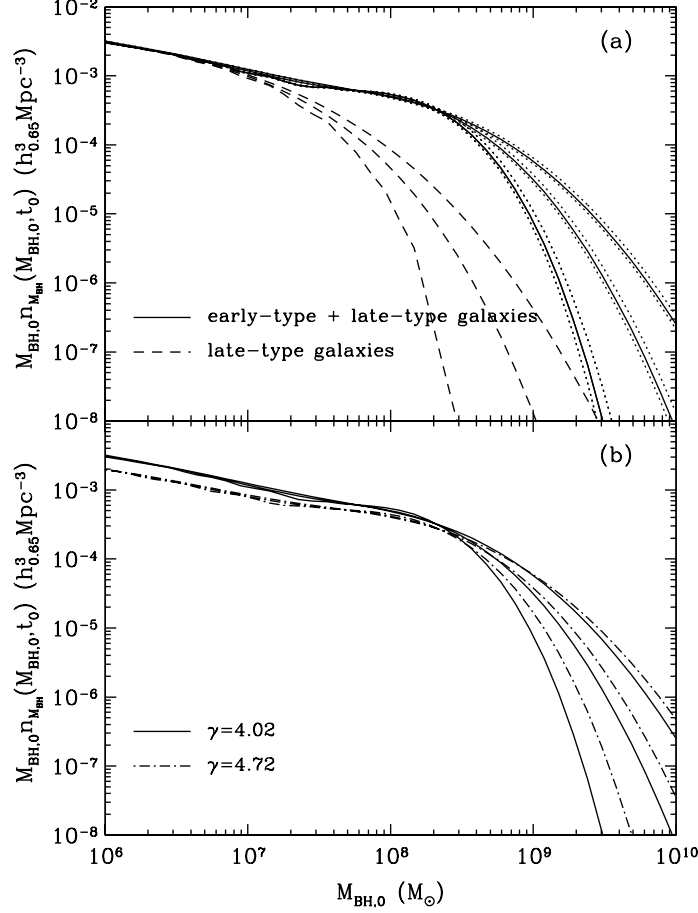


Fig. 1.— Local BHMF obtained from observations of the velocity dispersion distribution of nearby galaxies and the BH mass-velocity dispersion relation. (a) Solid lines represent the  $M_{\text{BH},0} n_{M_{\text{BH}}}(M_{\text{BH},0}, t_0)$  in both early-type and late-type galaxies (see eq. 38–44); dashed lines represent the  $M_{\text{BH},0} n_{M_{\text{BH}}}(M_{\text{BH},0}, t_0)$  in late-type galaxies. Different solid or dashed lines are obtained with different values of the intrinsic scatter  $\Delta_{\log M_{\text{BH},0}}$  ( $=0, 0.27$ , and  $0.4$  dex from bottom to top at the high-mass end, respectively) in the  $M_{\text{BH},0} - \sigma$  relation (eq. 42). The two dotted lines adjacent to each solid line give the effect of the  $1-\sigma$  error of the best-fit parameters in the velocity-dispersion function of early-type galaxies (eq. 39). (a) shows that the local BHMF at the high-mass end ( $\gtrsim 3 \times 10^8 M_{\odot}$ ) is significantly affected by  $\Delta_{\log M_{\text{BH},0}}$ , and the uncertainty of the BHMF due to the uncertainty in the velocity-dispersion function of early-type galaxies is negligible compared to the uncertainty due to the intrinsic scatter  $\Delta_{\log M_{\text{BH},0}}$  in the  $M_{\text{BH},0} - \sigma$  relation. (b) Solid lines are the same as those in (a), which are obtained with the slope  $\gamma = 4.02$  in relation (42) (Tremaine et al. 2002), while the dot-dashed lines are obtained with  $\gamma = 4.72$  (Merritt & Ferrarese 2001). The difference of the BHMF at the high-mass end due to the difference in  $\gamma$  is not as significant as that due to the difference of the intrinsic scatter  $\Delta_{\log M_{\text{BH},0}}$  in the  $M_{\text{BH},0} - \sigma$  relation. See details in § 3.1.3.

Boyle et al. (2000) use the function form of equation (45) to fit a much larger data set from the 2dF QSO redshift survey (Boyle et al. 2000) and Large Bright QSO survey (Hewett, Foltz & Chaffee 1995), which contain over 6000 QSOs, and give the QSOLF with absolute magnitudes  $-26 < M_B < -23$  and redshift  $0.35 < z < 2.3$  in our standard cosmological model  $(\Omega_m, \Omega_\Lambda) = (0.3, 0.7)$  by the following parameters:

$$\Psi_M^* = 2.9 \times 10^{-6} h^3 \text{Mpc}^{-3} \text{mag}^{-1}, \quad (51)$$

$$M_B^*(z) = M_B^*(0) - 2.5(k_1 z + k_2 z^2), \quad (52)$$

$$M_B^*(0) = -21.14 + 5 \log h, k_1 = 1.36, k_2 = -0.27, \quad (53)$$

$$\beta_1 = -1.58 \text{ and } \beta_2 = -3.41. \quad (54)$$

The quadratic dependence of the characteristic magnitude  $M_B^*(z)$  on  $z$  in equations (48) and (52) shows an increasing characteristic luminosity with increasing redshift at low redshift ( $z \lesssim 2.5$ ) and a decline of the characteristic luminosity at higher redshift, which is suggested by observations (e.g. Shaver et al. 1996), although the LF is not yet accurate enough to confirm the decline at  $z > 2.5$ .

The QSOLF over the range  $3.6 < z < 6$  provided in Fan et al. (2001, 2003) gives a flatter bright-end slope ( $\beta_2 = -2.5$ ) than equations (50) and (54); however, in our calculation below, we simply extrapolate equations (50) and (54) to high redshift because the detailed QSOLF at  $z > 3.5$  does not affect our results much (see Fig. 2 below; if we use the LF in Fan et al. 2001, our results change by less than a few percent).

Using equations (45)–(54), we obtain the time integral of the LF of optically bright QSOs

$$\mathcal{T}_{M_B, \text{QSO}}^{\text{opt}}(M_B, t_0) \equiv \int_0^\infty \Psi_{M_B, \text{QSO}}^{\text{opt}}(M_B, t) dt = 0.92 L_B \mathcal{T}_{L_B, \text{QSO}}^{\text{opt}}(L_B, t_0) \quad (55)$$

as a function of the absolute magnitude  $M_B$  shown in Figure 2. Both of the results obtained from the QSOLFs given by Boyle et al. (2000; shown as solid lines; eqs. 47–50) and those given by Pei (1995; shown as dotted lines; eqs. 51–54) are presented. In the calculation, the QSOLFs are extrapolated to the parameter space not covered by the observations. In Figure 2a we show the integral of the QSOLF over time  $0 \leq z \leq 2.3$  as the bottom solid and dotted lines and the integral of the QSOLF over the whole cosmic time  $\mathcal{T}_{M_B, \text{QSO}}^{\text{opt}}(M_B, t_0)$  as the top solid and dotted lines. As seen from panel (a), the difference of the time integral of the QSOLF due to different versions of QSOLFs is negligible. In Figure 2b we show the fraction of  $\mathcal{T}_{M_B, \text{QSO}}^{\text{opt}}(M_B, t_0)$  contributed by QSOs in the range  $0 \leq z \leq 2.3$  (bottom solid and dotted lines), which is more than 50% at  $M_B > -26$  and 75% at  $M_B > -23$ , and we also show the fraction contributed by QSOs in the range  $0 \leq z \leq 3.5$  (top solid and dotted lines), which is more than 95% at any  $M_B$  in the figure. Thus, the effect of the uncertainty in the QSOLF at high redshift on the time integral of QSOLF can be neglected.

#### 4. Is the local BH mass function consistent with the QSO luminosity function?

With the goal to obtain accurate observational constraints on the QSO luminosity evolution and the fundamental parameters of the QSO model (see § 2.4), we compare the time-integral of the QSOLF with that predicted from local BHs in this section (see eq. 21 in § 2.2 and inequalities 60 and 62 below). Note that the luminosity in the assumed model on the QSO luminosity evolution in § 2.4 is the bolometric luminosity  $L_{\text{bol}}$ . However, the QSOLF obtained from observations is usually in a specific band (which is the  $B$  band in this paper). Before the comparison, we first transfer the bolometric luminosity to the luminosity in a specific band.

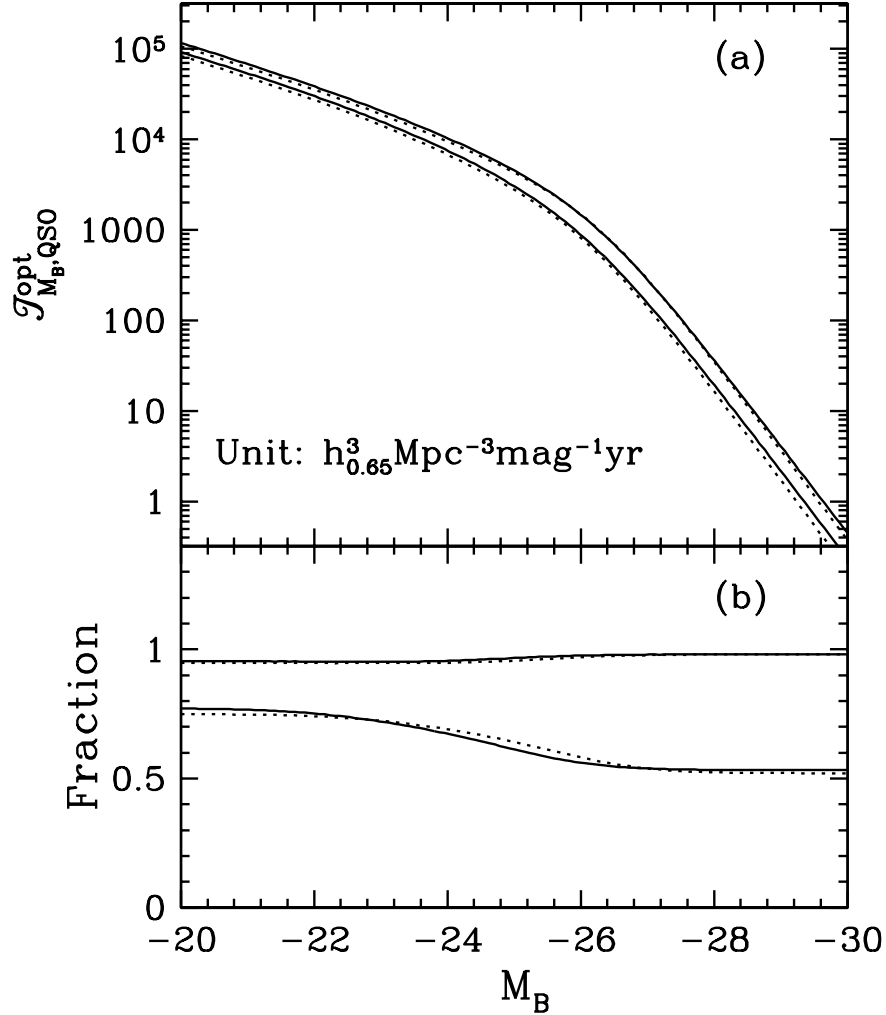


Fig. 2.— Time integral of the LF of optically bright QSOs as a function of the absolute magnitude  $M_B$  (see eq. 55). The results obtained by using the QSOLFs given by Pei (1995) (eqs. 47–50) are shown as dotted lines, and those obtained by using the QSOLFs given by Boyle et al. (2000) (eqs. 51–54) are shown as solid lines. The redshift range of the QSOLF is only  $0.35 < z < 2.3$  for Boyle et al. (2000) and  $0.1 < z < 4.5$  for Pei (1995). In the calculations, both are extrapolated to the parameter space not covered by the observations. (a) Top solid and dotted lines represent the integral of the QSOLF over the whole cosmic time  $\mathcal{T}_{M_B, \text{QSO}}^{\text{opt}}(M_B, t_0)$ ; bottom solid and dotted lines represent the integral of the QSOLF over time in the redshift range  $0 \leq z \leq 2.3$ . The difference due to different versions of the QSOLFs is negligible. (b) Top solid and dotted lines give the fraction of  $\mathcal{T}_{M_B, \text{QSO}}^{\text{opt}}(M_B, t_0)$  contributed by the QSOs with redshift  $0 \leq z \leq 3.5$ ; bottom solid and dotted lines give the fraction contributed by the QSOs with redshift  $0 \leq z \leq 2.3$ . This figure shows that the effect due to the uncertainty of the QSOLF at high redshift on the time integral of QSOLF can be neglected. See § 3.2.

#### 4.1. The bolometric correction

We denote  $C_B$  as the bolometric correction in the  $B$  band, defined through  $L_{\text{bol}} \equiv C_B L_{\nu_B}$ , where  $L_{\nu_B}$  is the energy radiated at the central frequency of the  $B$  band per unit time and logarithmic interval of frequency. We assume that  $C_B$  is independent of the cosmic time  $t$ . We denote  $P(C_B|L_{\text{bol}})$  as the probability distribution function of the bolometric correction  $C_B$  at a given  $L_{\text{bol}}$ . Thus, we have the LF of the progenitors of local BHs in the  $B$  band as follows:

$$n_{L_{\nu_B}}(L_{\nu_B}, t) = \int C_B P(C_B|L_{\text{bol}}) n_{L_{\text{bol}}}(L_{\text{bol}}, t) dC_B. \quad (56)$$

With equations (18) and (56), we have

$$\mathcal{T}_{L_{\nu_B}, \text{local}}(L_{\nu_B}, t_0) \equiv \int_0^\infty n_{L_{\nu_B}}(L_{\nu_B}, t) dt = \int C_B P(C_B|L_{\text{bol}}) \mathcal{T}_{L_{\text{bol}}, \text{local}}(L_{\text{bol}}, t_0) dC_B. \quad (57)$$

Similar to equation (21), we have

$$\mathcal{T}_{L_{\nu_B}, \text{QSO}}(L_{\nu_B}, t_0) = \mathcal{T}_{L_{\nu_B}, \text{local}}(L_{\nu_B}, t_0); \quad (58)$$

and according to equation (55), we have

$$\mathcal{T}_{M_B, \text{QSO}}(M_B, t_0) = \mathcal{T}_{M_B, \text{local}}(M_B, t_0). \quad (59)$$

Considering that QSOs in the equation above include both optically bright QSOs and obscured QSOs, we have

$$\mathcal{T}_{M_B, \text{QSO}}^{\text{opt}}(M_B, t_0) \leq \mathcal{T}_{M_B, \text{local}}(M_B, t_0). \quad (60)$$

The ratios of the time integral of the QSOLF and that predicted from the local BHMF are given as follows:

$$\mathcal{R}(M_B, t_0) \equiv \frac{\mathcal{T}_{M_B, \text{local}}(M_B, t_0)}{\mathcal{T}_{M_B, \text{QSO}}(M_B, t_0)} = 1 \quad (61)$$

and

$$\mathcal{R}^{\text{opt}}(M_B, t_0) \equiv \frac{\mathcal{T}_{M_B, \text{local}}(M_B, t_0)}{\mathcal{T}_{M_B, \text{QSO}}^{\text{opt}}(M_B, t_0)} \geq 1. \quad (62)$$

The value of  $\mathcal{R}^{\text{opt}}(M_B, t_0) - 1$  gives the number ratio of obscured QSOs to optically bright QSOs.

Elvis et al. (1994) study the spectral energy density distribution of a sample of 47 QSOs and find that the bolometric corrections in the  $B$  band have a mean value  $\overline{C}_B = 11.8$  with standard deviation  $\Delta_{C_B} = 4.3$ . The origin of the non-uniform of the bolometric correction (or the spectral energy distribution) is not yet clear, which could be due to the difference in the accretion rate, the BH mass and spin, etc. For example, with increasing BH mass, the bolometric correction in the  $B$  band may decrease since the peak of its spectral energy distribution may move from a short wavelength toward the  $B$  band or long wavelength, and with increasing accretion rate, the bolometric correction in the  $B$  band may decrease since it may have a softer spectrum in the X-ray band. In this paper, for simplicity, we assume that the probability distribution function of the bolometric correction  $P(C_B|L_{\text{bol}})$  is independent of  $L_{\text{bol}}$  and follows a Gaussian distribution as follows:

$$P(C_B|L_{\text{bol}}) = \frac{1}{\sqrt{2\pi}\Delta_{C_B}} \exp \left[ -\frac{(C_B - \overline{C}_B)^2}{2\Delta_{C_B}^2} \right]. \quad (63)$$

In the study below we use two values of  $\Delta_{C_B} = 4.3$  and 0 [ $P(C_B|L_{\text{bol}}) = \delta(C_B - \overline{C}_B)$  if  $\Delta_{C_B} = 0$ ] to check the effect of uncertainties in the distribution of the bolometric corrections.



Note that inequalities (60) and (62) can be generalized to other bands (e.g., the X-ray band). Given the observed QSOLF and the bolometric correction in some other bands, it is worthy to make similar comparisons as is done in the B band below (see also discussion in § 5.2).

## 4.2. Observational constraints on the nuclear/QSO luminosity evolution and BH growth

In § 2.4, the model of the nuclear/QSO luminosity evolution is characterized by three parameters: the period of the nuclear activity in the first phase  $\tau_1$ , the characteristic luminosity declining timescale in the second phase  $\tau_D$ , and the efficiency  $\epsilon$ . In § 4.2.1, using inequality (60) or (62) (see also eq. 21), we compare  $\mathcal{T}_{M_B, \text{QSO}}^{\text{opt}}(M_B, t_0)$  with  $\mathcal{T}_{M_B, \text{local}}(M_B, t_0)$  obtained with different values of  $\tau_1/\tau_{\text{Sp}}$ ,  $\tau_D/\tau_{\text{Sp}}$ , and  $\epsilon$  to provide observational constraints on the QSO model and BH growth. In the figures of this section, the results are shown in the luminosity range  $-20 > M_B > -30$ . However, the results are fairly secure probably only in the range  $-23 \gtrsim M_B \gtrsim -26$  (Boyle et al. 2000) (which are marked by two vertical thin dot-dashed lines in the figures), and the results at  $M_B \lesssim -26$  might be affected by the uncertainty of the small number statistics. In § 4.2.3, we show the effects of the uncertainty of the intrinsic scatter of the BH mass–velocity dispersion relation of local galaxies and the scatter of the bolometric correction of QSOs ( $\Delta_{\log M_{\text{BH},0}}$  and  $\Delta_{C_B}$ ).

### 4.2.1. $\tau_1/\tau_{\text{Sp}}$ , $\tau_D/\tau_{\text{Sp}}$ , $\epsilon$ , and the obscuration ratio

In this subsection we always set  $\Delta_{\log M_{\text{BH},0}} = 0.27 \text{ dex}$  (Tremaine et al. 2002) and  $\Delta_{C_B} = 4.3$  (Elvis et al. 1994). With the luminosity evolution described in § 2.4, below we study three models: in model (a), only the first (or “demand limited”) phase is considered; in model (b), only the second (or supply limited) phase is considered; and in model (c), both the first and the second phases are considered.

In model (a),  $\tau_D = 0$  and  $\tau_1$  is a free parameter (see eq. 30). We first show the result obtained by setting  $\epsilon = 0.1$  in Figure 3 and then see the change of the result by changing the value of  $\epsilon$  in Figure 4.

- In Figure 3a,  $\mathcal{T}_{M_B, \text{local}}(M_B, t_0)$  is shown as the dashed lines, and  $\mathcal{T}_{M_B, \text{QSO}}^{\text{opt}}(M_B, t_0)$  is shown as the solid line; and their ratios  $\mathcal{R}^{\text{opt}}(M_B, t_0)$  are shown as the dashed lines in panel (b). As seen from Figure 3(a) and (b),  $\mathcal{T}_{M_B, \text{local}}(M_B, t_0)$  and  $\mathcal{R}^{\text{opt}}(M_B, t_0)$  increase with increasing  $\tau_1/\tau_{\text{Sp}}$  ( $= 0.3, 1, 4$  from bottom to top at the faint end, respectively). The reason of the increasing is that increasing  $\tau_1/\tau_{\text{Sp}}$  will increase the mass range (or the upper limit of the mass range) of local BHs that had nuclear luminosity  $L$  in their evolution history (see eqs. 18 and 36). In this model, we get the following constraints:
  - (i) Constraints on  $\tau_1/\tau_{\text{Sp}}$  from the sensitivity of  $\mathcal{T}_{M_B, \text{local}}(M_B, t_0)$  to  $\tau_1/\tau_{\text{Sp}}$ : as seen from Figure 3(a), if  $\tau_1/\tau_{\text{Sp}} \gtrsim 1$ ,  $\mathcal{T}_{M_B, \text{local}}(M_B, t_0)$  becomes insensitive to the value of  $\tau_1/\tau_{\text{Sp}}$  at  $M_B \lesssim -26$ . Our calculations also show that if  $\tau_1/\tau_{\text{Sp}} \gtrsim 4$ ,  $\mathcal{T}_{M_B, \text{local}}(M_B, t_0)$  becomes insensitive to the values of  $\tau_1/\tau_{\text{Sp}}$  at  $M_B \lesssim -23$ . For example, we have  $\mathcal{T}_{M_B, \text{local}}(\tau_1/\tau_{\text{Sp}} = 10)/\mathcal{T}_{M_B, \text{local}}(\tau_1/\tau_{\text{Sp}} = 1) - 1 \lesssim 10\%$  at  $M_B \lesssim -26$  and  $\mathcal{T}_{M_B, \text{local}}(\tau_1/\tau_{\text{Sp}} = 10)/\mathcal{T}_{M_B, \text{local}}(\tau_1/\tau_{\text{Sp}} = 4) - 1 \lesssim 15\%$  at  $M_B \lesssim -23$ . The reason for this insensitivity is that the additional contribution to  $\mathcal{T}_{M_B, \text{local}}(M_B, t_0)$  at a given  $M_B$  due to the increase of  $\tau_1/\tau_{\text{Sp}}$  comes from the BHs at the high-mass end (see eqs. 18 and 36). Thus, for a given  $M_B$ , if  $\tau_1/\tau_{\text{Sp}}$  is larger than a certain value, the masses of the BHs from which the additional contribution comes will be significantly high, and the additional contribution may be negligible since the local BHMF decreases sharply (or exponentially) at the high-mass end ( $M_{\text{BH},0} \gtrsim 3 \times 10^8 M_\odot$ ). The insensitivity of  $\mathcal{T}_{M_B, \text{local}}(M_B, t_0)$  to the value of  $\tau_1/\tau_{\text{Sp}}$  above

suggests that if the real  $\tau_1/\tau_{\text{Sp}}$  is larger than 4, it is more likely that only the lower limit of  $\tau_1/\tau_{\text{Sp}}$  ( $\sim 4$  here), rather than an accurate value of  $\tau_1/\tau_{\text{Sp}}$ , can be provided by fitting  $\mathcal{T}_{M_B, \text{local}}(M_B, t_0)$  to  $\mathcal{T}_{M_B, \text{QSO}}(M_B, t_0)$ . To get an accurate estimate of  $\tau_1/\tau_{\text{Sp}}$ , it would require either observations at fainter luminosities or precise measurements of both the QSOLF and the local BHMF (e.g., with error much less than 10%) within the current luminosity range. The insensitivity of  $\mathcal{T}_{M_B, \text{local}}$  to  $\tau_1/\tau_{\text{Sp}}$  still holds if  $\tau_D$  is non-zero (see eqs. 33 and 36). The suggestion above will also not be affected by changing the value of  $\epsilon$ , since as will be seen below (Fig. 4), changing  $\epsilon$  does not affect the shape of  $\mathcal{T}_{M_B, \text{local}}(M_B, t_0)$  or  $\mathcal{R}^{\text{opt}}(M_B, t_0)$  for a given  $\tau_1/\tau_{\text{Sp}}$ .

- (ii) Constraints on  $\tau_1/\tau_{\text{Sp}}$  from the value of  $\mathcal{R}^{\text{opt}}(M_B, t_0)$ : Figure 3(b) shows that  $\mathcal{R}^{\text{opt}}(M_B, t_0)$  is significantly smaller than 1 if  $\tau_1/\tau_{\text{Sp}} \ll 1$  (see the bottom dashed line with  $\tau_1/\tau_{\text{Sp}} = 0.3$ ); and  $\mathcal{R}^{\text{opt}}(M_B, t_0)$  can roughly exceed or be around 1 at  $-23 \gtrsim M_B \gtrsim -26$  if  $\tau_1/\tau_{\text{Sp}} \gtrsim 1$  (see the middle and top dashed lines obtained with  $\tau_1/\tau_{\text{Sp}} = 1$  and 4). Thus, to satisfy inequality (62), the QSO lifetime should be  $\gtrsim \tau_{\text{Sp}} \simeq 5 \times 10^7 \text{ yr}$  if  $\epsilon \simeq 0.1$ . This conclusion will not be affected after setting a non-zero timescale  $\tau_D$ , since as will be seen below (Fig. 6), increasing  $\tau_D$  decreases  $\mathcal{R}^{\text{opt}}(M_B, t_0)$  at least at  $M_B \sim -26$ .
  - (iii) Constraints on the ratio of obscuration: as seen from Figure 3b, if  $\tau_1/\tau_{\text{Sp}} \gtrsim 4$ ,  $\mathcal{R}^{\text{opt}}(M_B, t_0)$  is about 2 at  $M_B \simeq -23$  and about 1 at  $M_B \simeq -26$ . This result suggests that if  $\tau_1/\tau_{\text{Sp}} \gtrsim 4$ , there should exist some obscured QSOs (which are missed by optical surveys), and the ratio of obscured QSOs to unobscured (or optically bright) QSOs may be about 1 at the faint end (intrinsic absolute magnitude  $M_B \sim -23$ ); compared to optically bright QSOs, few obscured QSOs are expected to exist at the luminous end ( $M_B \sim -26$ ). If  $\tau_1/\tau_{\text{Sp}} \simeq 1$ , few obscured QSOs/AGNs are expected to exist at both faint and bright ends. Note that these conclusions are obtained with  $\epsilon = 0.1$  and  $\tau_D = 0$ , and may be affected if  $\epsilon \gtrsim 0.1$  or  $\tau_D > 0$ .
- In Figure 4a and 4b, the dotted, dashed, and dot-dashed lines represent the results obtained with  $\epsilon = 0.057$  (the efficiency for the thin-disk accretion onto a Schwarzschild BH), 0.1, and 0.31 (the maximum efficiency allowed for the thin-disk accretion onto a Kerr BH with dimensionless spin parameter 0.998, see Thorne 1974; here we do not consider the possibility of extremely high efficiency, see, e.g., Narayan, Igumenshchev & Abramowicz 2003; Li & Paczyński 2000), respectively. As in Figure 3, for each type of those lines, we show the results obtained with  $\tau_1/\tau_{\text{Sp}} = 4, 1$ , and 0.3 (top, middle, and bottom lines, respectively). As seen from Figure 4,  $\mathcal{T}_{M_B, \text{local}}(M_B, t_0)$  and  $\mathcal{R}^{\text{opt}}(M_B, t_0)$  increase with increasing  $\epsilon$  without changing the shape (which can also be inferred from eqs. 31 and 35). We obtain the following constraints from Figure 4.
    - (i) Constraints on  $\epsilon$ : as seen from Figure 4(b), if  $\epsilon = 0.057$  (dotted lines),  $\mathcal{R}^{\text{opt}}(M_B, t_0)$  are generally smaller than 1, which suggests that the efficiency of QSOs/AGNs cannot be significantly less than 0.1.
    - (ii) Constraints on  $\tau_1/\tau_{\text{Sp}}$ : our calculations show that if  $\epsilon = 0.31$ , to satisfy inequality (62), it is required that  $\tau_1/\tau_{\text{Sp}} \gtrsim 0.2$  or the QSO lifetime should be  $\gtrsim 4 \times 10^7 \text{ yr}$  (see also the bottom dot-dashed line in Fig. 4b).
    - (iii) Constraints on the ratio of obscuration: as seen from Figure 4(b), if  $\epsilon = 0.31$  and  $\tau_1/\tau_{\text{Sp}} \gtrsim 4$  (see the top dot-dashed line),  $\mathcal{R}^{\text{opt}}(M_B, t_0)$  is  $\sim 8$  at  $M_B \sim -23$  and  $\sim 4$  at  $M_B \sim -26$ , which suggests that the upper limit of the ratio of obscured QSOs/AGNs to un-obscured QSOs/AGNs is  $\sim 7$  at  $M_B \sim -23$  and  $\sim 3$  at  $M_B \sim -26$ .

The constraints obtained above from Figure 4 will not be affected by having a non-zero  $\tau_D$ , since as will be seen below (Fig. 6), increasing  $\tau_D$  decreases the  $\mathcal{T}_{M_B, \text{local}}(M_B, t_0)$  or  $\mathcal{R}^{\text{opt}}(M_B, t_0)$  at least at  $M_B \sim -26$ .

In model (b),  $\tau_I = 0$  and  $\tau_D$  is a free parameter (see eq. 32). Setting  $\epsilon = 0.1$ , the results obtained with  $\tau_D/\tau_{\text{Sp}} = 0.3, 1$ , and 4 are shown as dashed lines from bottom to top at the faint end, respectively, in Figure 5. As seen from Figure 5, for any given  $\tau_D$ ,  $\mathcal{T}_{M_B, \text{local}}(M_B, t_0)$  is smaller than  $\mathcal{T}_{M_B, \text{QSO}}^{\text{opt}}(M_B, t_0)$  at  $M_B \lesssim -26$  at least by a factor of  $\sim 10$  if  $\epsilon = 0.1$  (and at least by a factor of 2 or 3 if  $\epsilon = 0.31$ ). This result suggests that to satisfy the expected relation between the QSOLF and local BHMF (inequalities 60 or 62), it is impossible to only have the luminosity-declining phase in the QSO luminosity evolution.

In model (c), both  $\tau_I$  and  $\tau_D$  are not zero. Setting  $\tau_I/\tau_{\text{Sp}} = 4, 1, 0.3$  and  $\epsilon = 0.1$ , we show the results obtained with  $\tau_D/\tau_{\text{Sp}} = 0.3$  and 1 as the dashed and dotted lines, respectively, in Figure 6. The value of  $\tau_D$  affects the shape and value of  $\mathcal{T}_{M_B, \text{local}}(M_B, t_0)$  and  $\mathcal{R}^{\text{opt}}(M_B, t_0)$ . As seen from Figures 3 and 6, increasing  $\tau_D/\tau_{\text{Sp}}$  decreases  $\mathcal{T}_{M_B, \text{local}}(M_B, t_0)$  and  $\mathcal{R}^{\text{opt}}(M_B, t_0)$  at high luminosities (e.g.,  $M_B \lesssim -26$ ). Figure 6b shows that at  $M_B \sim -26$ ,  $\mathcal{R}^{\text{opt}}(M_B, t_0)$  is significantly smaller than 1 (about 0.2–0.3 if  $\tau_D/\tau_{\text{Sp}} = 1$  and about 0.3–0.6 if  $\tau_D/\tau_{\text{Sp}} = 0.3$ ), which suggests that  $\tau_D$  should be significantly shorter than  $\tau_{\text{Sp}}$ , or the second (or supply limited) phase should not dominate the growth of local BHs (see eq. 33). Our calculation shows that this suggestion will not be significantly affected even if  $\epsilon = 0.31$ .

By combining the constraints obtained in the three models above, below we summarize the results on the fundamental parameters of the QSO luminosity evolution and BH growth:

1. The QSO mass-to-energy conversion efficiency is  $\epsilon \gtrsim 0.1$  (see Fig. 4).
2. The period of the nuclear activity is longer than  $\sim \tau_{\text{Sp}} \simeq 5 \times 10^7 \text{ yr}$  if  $\epsilon = 0.1$  and longer than  $\sim 0.2\tau_{\text{Sp}} = 4 \times 10^7 \text{ yr}$  if  $\epsilon = 0.31$  (see Figs. 3 and 4).
3. If the real  $\tau_I$  is larger than a certain value ( $\sim 4\tau_{\text{Sp}}$  here), it is difficult to provide an accurate estimate on the value of  $\tau_I$  unless observations are extended to fainter luminosities or precise measurements of both the QSOLF and the local BHMF within the current luminosity range are available (e.g., with error much less than 10%; see Fig. 3).
4. The characteristic declining timescale of the luminosity evolution in the second phase  $\tau_D$  should be significantly shorter than  $\tau_{\text{Sp}}$  (e.g.,  $\tau_D < 0.3\tau_{\text{Sp}}$  if  $\epsilon = 0.1$  and  $\tau_D < \tau_{\text{Sp}}$  if  $\epsilon = 0.31$ ; see Fig. 6); thus, the second phase does not dominate the growth of local BHs (see eq. 33).
5. There might exist a large number of obscured QSOs/AGNs, but the ratio of the obscured QSOs/AGNs to the unobscured (or optically bright) QSOs should be not larger than 7 at  $M_B \sim -23$  and 3 at  $M_B \sim -26$  if  $\epsilon \simeq 0.31$  (see the top dotted line in Fig. 4) and not larger than 1 at  $M_B \sim -23$  and negligible at  $M_B \sim -26$  if  $\epsilon = 0.1$  (see Fig. 3).

According to the results above, the lower limit of the QSO lifetime (defined directly through the luminosity evolution of individual QSOs) is  $\simeq 4 \times 10^7 \text{ yr}$ . There are also other independent methods (e.g., Martini 2003), such as the clustering of QSOs (Martini & Weinberg 2001; Haiman & Hui 2001) or the modeling of the QSOLF in hierarchical galaxy formation scenario (Kauffmann & Haehnelt 2000; Haiman & Loeb 1998), to provide constraints on the QSO lifetime (usually in the range of  $10^6 - 10^8 \text{ yr}$ ). Here we do not make a comparison with those results since the meanings of the QSO lifetime in different methods or contexts are

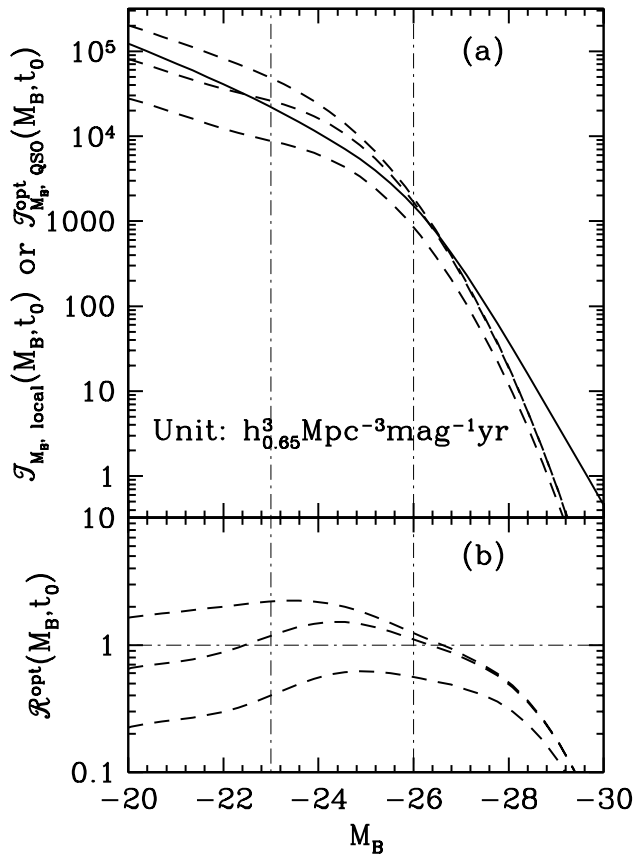


Fig. 3.— Time integral of the observed LF of optically bright QSOs and the time integral of the QSOLF predicted from local BHs. The model of the luminosity evolution of the nuclear activity in § 2.4 is used. The curves are obtained by setting the parameters  $\tau_D = 0$ ,  $\epsilon = 0.1$ ,  $\Delta_{\log M_{\text{BH},0}} = 0.27$  dex, and  $\Delta_{C_B} = 4.3$ . (a) Dashed lines represent the time integral of the QSOLF predicted from local BHs  $\mathcal{T}_{M_B, \text{local}}(M_B, t_0)$  (eqs. 18, 34, 35 and 57); solid line represents the time integral of the observed LF of optically bright QSOs  $\mathcal{T}_{M_B, \text{QSO}}^{\text{opt}}(M_B, t_0)$  (eqs. 45 and 55). (b) Ratio of the time integrals  $\mathcal{R}^{\text{opt}}(M_B, t_0)$  (eq. 62). The horizontal thin dot-dashed line represents  $\mathcal{R}^{\text{opt}}(M_B, t_0) = 1$ . The two vertical thin dot-dashed lines mark the region  $-23 < M_B < -26$  in which the LFs of optically bright QSOs are fairly secure (Boyle et al. 2000). In each panel, the dashed lines represent the results obtained with  $\tau_1/\tau_{\text{Sp}} = 0.3, 1$ , and  $4$  from bottom to top at the faint end, respectively. Inequality (62) implies that the dashed line should be consistent with the solid line in (a) or approximately equal to 1 in (b) if obscured QSOs are significantly less than optically bright QSOs, and the dashed line should be higher than the solid line in (a) or higher than 1 in (b) if obscured QSOs are significantly numerous compared to optically bright QSOs. To satisfy inequality (62), the QSO lifetime  $\tau_1$  is required to be  $\gtrsim \tau_{\text{Sp}} \simeq 5 \times 10^7$  yr (if  $\epsilon \simeq 0.1$ ). See more discussion in § 4.2.1.

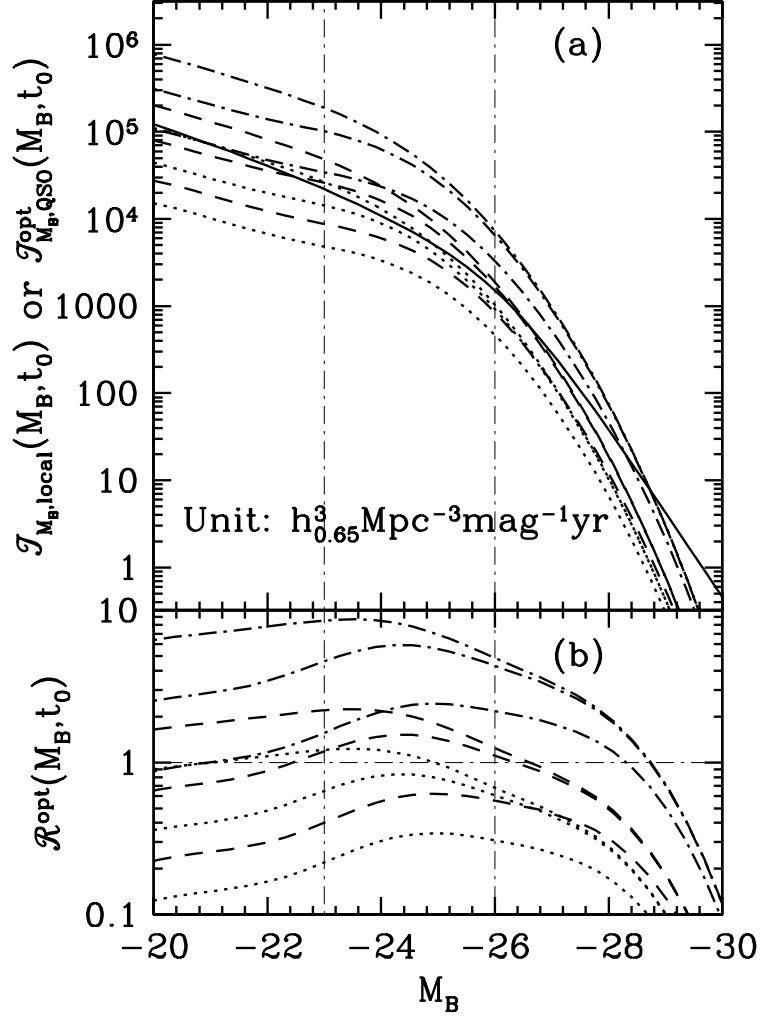


Fig. 4.— Same as Figure 3, except that there are additional results obtained with  $\epsilon = 0.057$  and  $0.31$  (not only  $\epsilon = 0.1$  in Fig. 3) shown as the dotted and dot-dashed lines, respectively. The curves shift upward with increasing  $\epsilon$ . As seen from (b), generally or at least at  $M_B < -25$ ,  $\mathcal{R}^{\text{opt}}(M_B, t_0)$  obtained with  $\epsilon = 0.057$  (dotted lines) are smaller than 1, which suggests that  $\epsilon$  cannot be significantly smaller than 0.1. See more discussion in § 4.2.1.

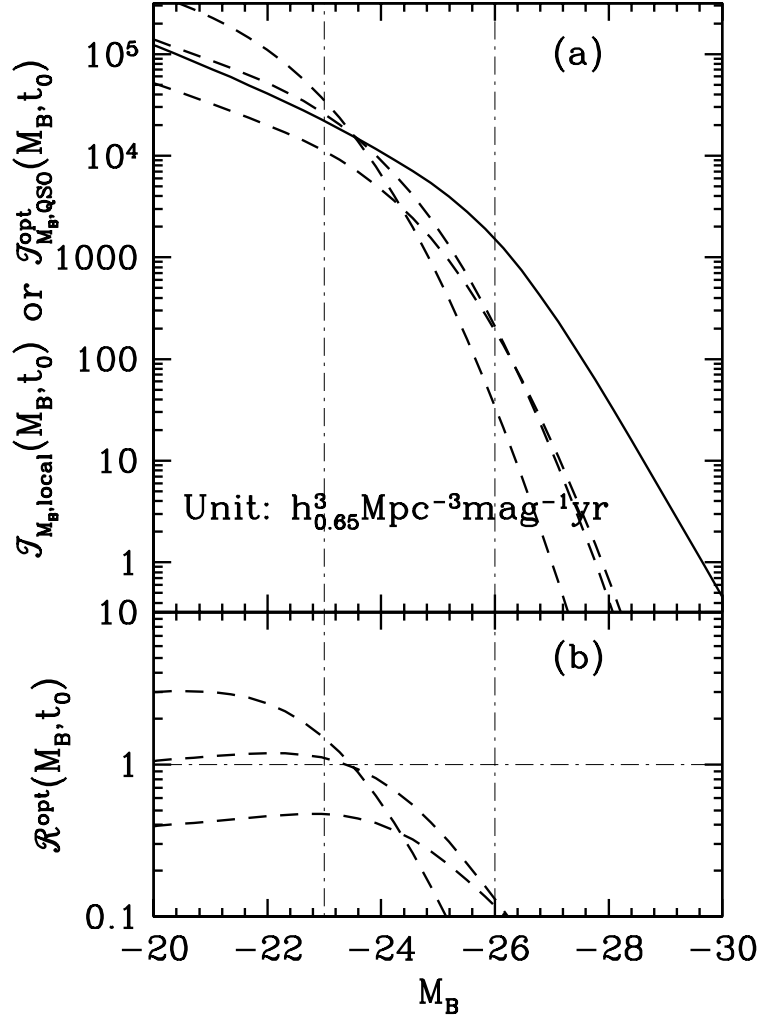


Fig. 5.— Same as Figure 3, but with  $\tau_I = 0$  and  $\tau_D/\tau_{\text{Sp}} = 4, 1$ , and  $0.3$  (from top to bottom at the faint end, respectively; dashed lines; model [b]). (b)  $\mathcal{R}^{\text{opt}}(M_B \sim -26)$  is significantly smaller than 1 (which is still true even if  $\epsilon = 0.31$ ). This figure suggests that to satisfy inequalities (60) and (62), it is impossible to only have the luminosity-declining phase (eq. 32, the second phase described in § 2.4) in the QSO luminosity evolution. See § 4.2.1.

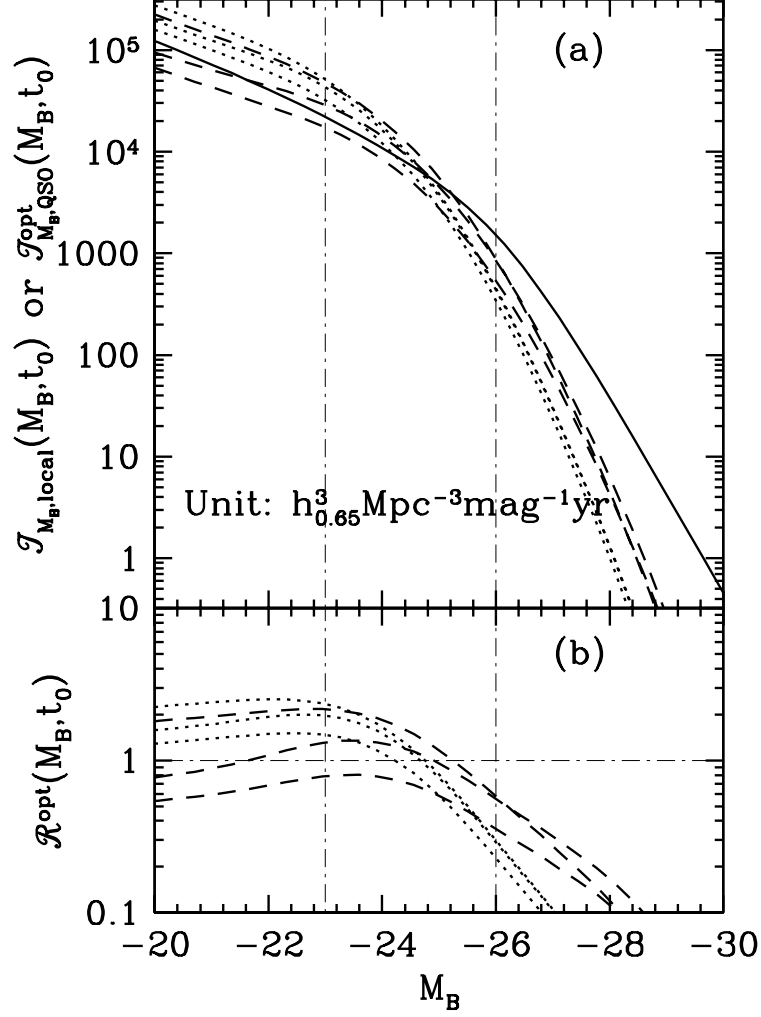


Fig. 6.— Same as Figure 3, but with  $\tau_D/\tau_{\text{Sp}} = 0.3$  (dashed lines) and 1 (dotted lines; model [c]). (b)  $\mathcal{R}^{\text{opt}}(M_B \sim -26)$  is significantly smaller than 1, which suggests that to satisfy inequalities (60) and (62),  $\tau_D$  should be significantly shorter than  $\tau_{\text{Sp}}$  (e.g.,  $\tau_D < 0.3\tau_{\text{Sp}}$ ), or the luminosity-declining phase (the second phase described in § 2.4) should not dominate the growth of local BHs. See § 4.2.1.

not exactly the same. The upper limit of the lifetime can be usually constrained by the rising and falling of the characteristic luminosity of the entire QSO population as a function of cosmic time (roughly a few times  $10^9$  yr; see eqs. 48 and 52).

It is worthy to note that item 3 above would hold for many other methods to estimate the QSO lifetime by using the QSOLF, not only for the specific study in this paper, as a result of the sharp decrease of the QSOLF at the bright end and the limited luminosity range of the observations.

Item 5 above does not exclude the possibility of the existence of a large number of obscured QSOs at high luminosities if the efficiency is high (e.g.,  $\epsilon \sim 0.3$ ), which is slightly different from the result obtained by comparing partial mass densities (see eq. 29) in Yu & Tremaine (2002) that obscured accretion is not important for the growth of high-mass BHs ( $> 10^8 M_\odot$ ). The reason for the difference is partly because, in the present study, we adopt a high value of  $\Delta_{\log M_{\text{BH},0}} (= 0.27 \text{ dex})$  and include the effect of the scatter of the bolometric corrections (for the detailed effects of  $\Delta_{\log M_{\text{BH},0}}$  and  $\Delta_{C_B}$  see § 4.2.3 and Figs. 8 and 9 below). Furthermore, Yu & Tremaine (2002) compare the partial mass density accreted in QSOs having luminosity higher than a certain value with the partial mass density in local BHs (see eq. 29), and the present study compares the number density (or the time-integral of the number density) at a given luminosity; hence, the result of the obscuration obtained in Yu & Tremaine (2002) is mainly for the ratio of all the BH *mass* accreted in obscured QSOs with intrinsic luminosity higher than a certain value, rather than the *number* ratio of obscured QSOs at a given luminosity in the present study.

In addition, in Figures 3–6 ( $\epsilon \lesssim 0.31$ ), inequalities (60) and (62) are always not satisfied at the bright end  $M_B \lesssim -29 - -26$ , which is mainly because the local BHMF declines more sharply than the QSOLF at the bright end (note that the velocity dispersion function of early-type galaxies is fitted by an exponential form at the bright end, but the QSOLF is fitted by a power law). The forms of the QSOLF and local BHMF at the bright end are probably affected by the uncertainty of the small number statistics; otherwise, the physical mechanism/parameters (e.g., QSO efficiency) of very luminous QSOs ( $M_B \lesssim -29 - -26$ ) or the properties of nearby galaxies with very big BHs ( $\gtrsim 10^9 M_\odot$ ) should be very different from those of the main population of QSOs or nearby early-type galaxies.

#### 4.2.2. Is it possible that most QSOs radiate at super-Eddington luminosities?

In § 2.4 it is assumed that after the nuclear activity is triggered, QSOs first radiate at the Eddington luminosity for a period  $\tau_1$  and then radiate at sub-Eddington luminosities as a result of the decline of available accretion material supply. However, accretion with super-Eddington luminosities might occur in some cases. For example, when BH mass is small and the accretion rate is sufficiently high, the outflow pushed by the radiation may be trapped by the infalling gas and the energy is radiated away at a rate higher than the Eddington limit (see discussion in Blandford 2003), or when some strong density inhomogeneity is developed in a thin disk, the disk may also radiate at super-Eddington luminosity (Begelman 2002).

Below we will see whether the expected relations given by equations (60) and (62) can be satisfied if all QSOs radiate at a luminosity higher than the Eddington luminosity, say, by a factor of  $l > 1$ . Note that in this case the value of the characteristic increasing timescale of the luminosity or BH mass, denoted by  $\tau'_{\text{Sp}}$ , is smaller than the value in equation (31) by a factor of  $l$ . In Figure 7 we show the time integral of the LFs obtained with  $\tau_1/\tau'_{\text{Sp}} = 4, 1, 0.3$  (from top to bottom) and with  $l = 2$  (dashed lines) and  $l = 5$  (dotted lines). The other parameters (such as  $\tau_D = 0$ ,  $\epsilon = 0.1$ , etc.) in Figure 7 are the same as those in Figure 3. As seen from Figure 7(b), at  $-23 > M_B > -26$ , either  $\mathcal{R}^{\text{opt}}(M_B, t_0)$  is smaller than 1, which is



inconsistent with inequality (62), or  $\mathcal{R}^{\text{opt}}(M_B, t_0)$  increases with increasing luminosity, which is inconsistent with current observations that few type II QSOs are observed and most observed obscured AGNs are at low luminosities (e.g., Barger et al. 2003). The results above suggest that it is unlikely that most QSOs radiate at a luminosity much higher than the Eddington luminosity (or accrete at an accretion rate much higher than the Eddington accretion rate). We expect that accretion with super-Eddington luminosities operates maybe only at the very early stage of the nuclear activity, and will not significantly affect our results obtained in § 4.2.

#### 4.2.3. Effects of the uncertainty of $\Delta_{\log M_{\text{BH},0}}$ and $\Delta_{C_B}$

The effect of the uncertainty of  $\Delta_{\log M_{\text{BH},0}}$  is shown in Figure 8. In Figure 8 we show  $\mathcal{T}_{M_B, \text{local}}(M_B, t_0)$  and  $\mathcal{R}^{\text{opt}}(M_B, t_0)$  obtained by setting  $\Delta_{\log M_{\text{BH},0}} = 0$  (dot-dashed lines) and 0.4 dex (dotted lines), as well as the results obtained in Figure 3 (shown by the dashed lines with  $\Delta_{\log M_{\text{BH},0}} = 0.27$  dex and the solid line). The other parameters of the dot-dashed and the dotted lines are the same as in Figure 3. As seen from Figure 8(b), the effect of the uncertainty of  $\Delta_{\log M_{\text{BH},0}}$  is negligible at  $M_B \gtrsim -24$ ; however,  $\mathcal{R}^{\text{opt}}(M_B, t_0)$  or  $\mathcal{T}_{M_B, \text{local}}(M_B, t_0)$  is significantly affected by the value of  $\Delta_{\log M_{\text{BH},0}}$  at  $M_B \gtrsim -26$ . For example, at  $M_B = -26$ ,  $\mathcal{R}^{\text{opt}}(M_B, t_0)$  obtained with  $\Delta_{\log M_{\text{BH},0}} = 0.4$  dex (dotted lines) is larger than that obtained with  $\Delta_{\log M_{\text{BH},0}} = 0.27$  dex (dashed lines) by a factor of  $\sim 2$  and is larger than that obtained with  $\Delta_{\log M_{\text{BH},0}} = 0$  (dot-dashed lines) by a factor of more than  $\sim 4$ .

The effect of the uncertainty of  $\Delta_{C_B}$  is shown in Figure 9. In Figure 9 we show the results obtained by setting  $\Delta_{C_B} = 0$  as the dotted lines, as well as those obtained in Figure 3 (dashed lines;  $\Delta_{C_B} = 4.3$ ). The other parameters of the dotted lines are the same as in Figure 3. As seen from Figure 9(b), at the faint end ( $M_B \lesssim -24$ ),  $\mathcal{R}^{\text{opt}}(M_B, t_0)$  [or  $\mathcal{T}_{M_B, \text{local}}(M_B, t_0)$ ] is insensitive to the value of  $\Delta_{C_B}$ ; however, at the luminous end ( $M_B \lesssim -26$ ),  $\mathcal{R}^{\text{opt}}(M_B, t_0)$  obtained with  $\Delta_{C_B} = 4.3$  (dashed lines) is larger than that obtained with  $\Delta_{C_B} = 0$  (dotted lines; e.g., by a factor of about 3 at  $M_B = -27$ ).

The results above raise the importance of accurately measuring both  $\Delta_{\log M_{\text{BH},0}}$  and  $\Delta_{C_B}$  and of studying the dependence of the bolometric correction on the BH mass, the accretion rate, or other physical parameters for precise understanding of the relation between the local BHMF and the QSOLF (especially at the luminous end, e.g.,  $M_B \lesssim -26$ ), the luminosity evolution of the nuclear activity, and the BH growth.

## 5. Discussions

### 5.1. The QSO luminosity evolution and the triggering history of the accretion onto seed BHs

As part of the steps to understand the physics behind the QSO phenomenon and BH growth, it is important to investigate both the luminosity evolution and the triggering history of the accretion onto their seed BHs, which together control the shape and the value of the QSOLF (see eqs. 2 and 9). In the currently popular coevolution scenario of QSOs and galaxy spheroids in the cold dark matter (CDM) cosmology, it is generally assumed that QSOs are triggered by hierarchical (major) mergers of galaxies, and the triggering rate is controlled by the (major) merger rate of galaxies (or halos in less fine models; e.g., Kauffmann & Haehnelt 2000; Haiman & Loeb 1998 and references therein). With an assumed luminosity evolution (e.g., usually a step function or an exponentially declining function in those models), the coevolution models can reproduce

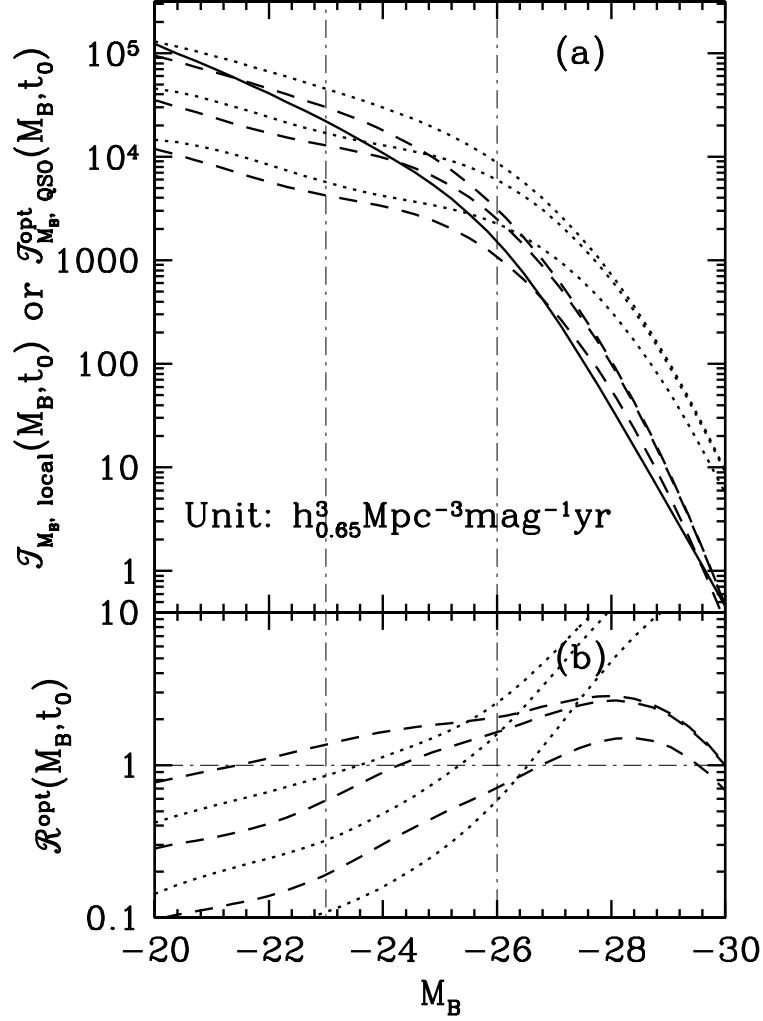


Fig. 7.— Same as Figure 3, except that the QSOs are assumed to radiate at a luminosity higher than the Eddington luminosity by a factor of  $l$  ( $\tau'_{\text{Sp}} = l^{-1}\tau_{\text{Sp}}$ ,  $\tau_{\text{I}}/\tau'_{\text{Sp}} = 4, 1, 0.3$ ,  $\tau_{\text{D}} = 0$ , and  $\epsilon = 0.1$ ). The dashed lines show the results obtained with  $l = 2$ , and the dotted lines show the results obtained with  $l = 5$ . As seen from (b), at  $-23 > M_B > -26$ ,  $\mathcal{R}^{\text{opt}}(M_B, t_0)$  either is smaller than 1, which is inconsistent with inequality (62), or increases with increasing luminosity, which is inconsistent with current observations on obscured AGNs (e.g., Barger et al. 2003). This figure suggests that it is unlikely that most QSOs radiate at a luminosity much higher than the Eddington luminosity (or accrete at an accretion rate much higher than the Eddington accretion rate). See details in § 4.2.2.

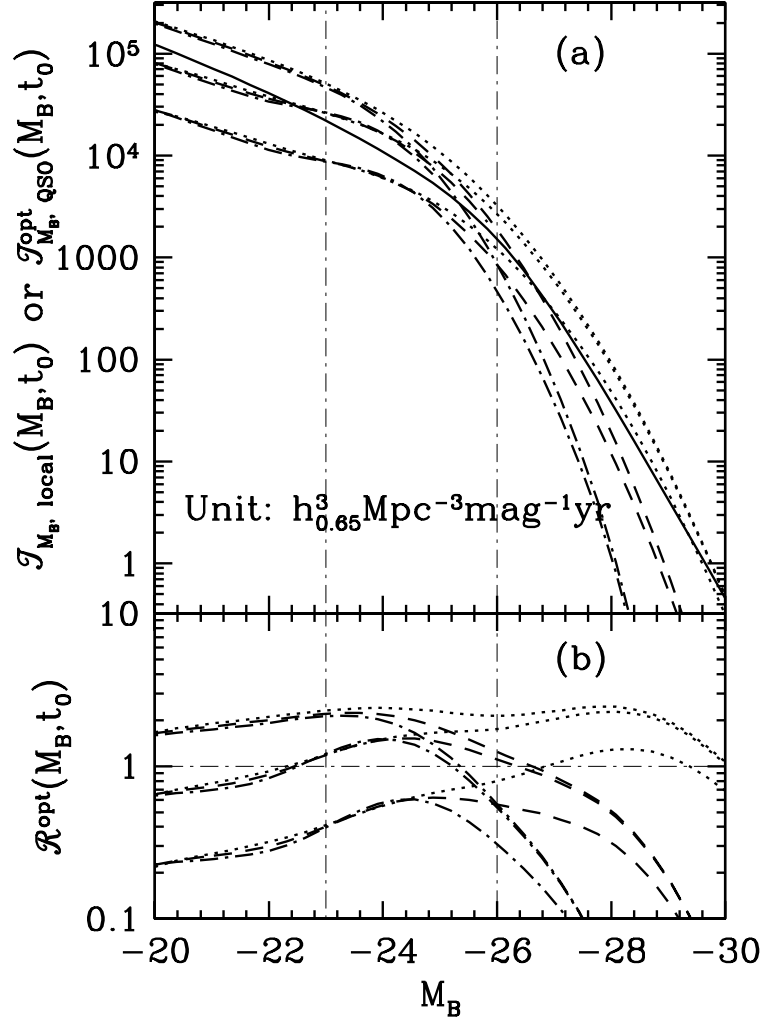


Fig. 8.— Same as Figure 3, except that there are additional results obtained with  $\Delta_{\log M_{\text{BH},0}} = 0$  and 0.4 dex (not only  $\Delta_{\log M_{\text{BH},0}} = 0.27$  dex in Fig. 3) shown as the dot-dashed and dotted lines, respectively. The effect of the uncertainty of  $\Delta_{\log M_{\text{BH},0}}$  is negligible at the faint end ( $M_B \gtrsim -24$ ) but may be significant at the bright end ( $M_B \lesssim -26$ ). See § 4.2.3.

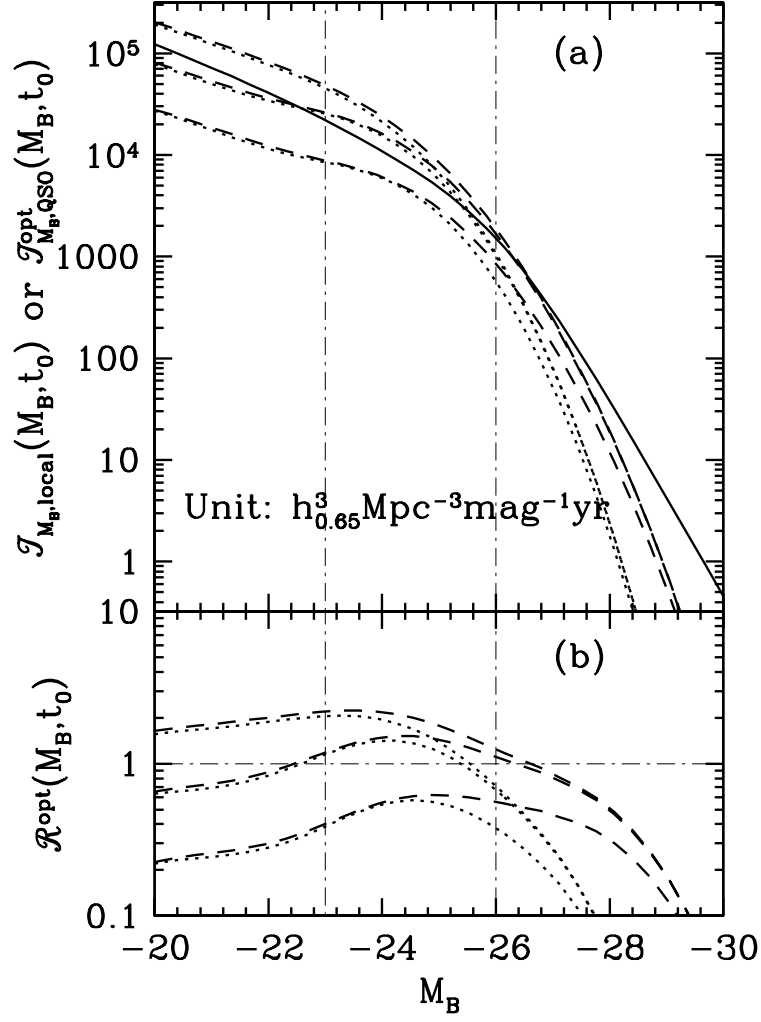


Fig. 9.— Same as Figure 3, except that there are additional results obtained with  $\Delta_{C_B} = 0$  (not only  $\Delta_{C_B} = 4.3$  in Fig. 3) shown as the dotted lines. The effect of the uncertainty of  $\Delta_{C_B}$  is negligible at the faint end ( $M_B \gtrsim -24$ ) but may be significant at the bright end ( $M_B \lesssim -26$ ). See § 4.2.3.

the observed QSOLF. However, in those models, as a result of many uncertainties in the estimate of the galaxy merger rate and the gas infalling rate for BH growth, it is hard to differentiate whether the change of the QSOLF is due to a change of the nuclear luminosity evolution or to a change of the triggering rate; hence, it is hard to give an accurate constraint on the QSO luminosity evolution. For example the QSOLF can be reproduced for a large range of the assumed lifetime ( $10^6$  to  $10^8$  yr; e.g. Kauffmann & Haehnelt 2000; Haiman & Loeb 1998).

In this paper, by investigating the relation between the QSOLF and the local BHMF, we separate the luminosity evolution of individual QSOs from the triggering rate of the QSO population, with the assumption that each local massive BH has experienced the QSO phases and BH mergers are ignored. As shown in equations (18) and (21), the triggering rate is circumvented, and only the luminosity evolution of individual QSOs is implicitly reflected by their lifetime  $\tau_{\text{life}}(M_{\text{BH},0})$  and the luminosity probability distribution  $P(L|M_{\text{BH},0})$  in their evolution history. Thus, the constraints on the QSO luminosity evolution (such as the QSO lifetime and the efficiency) obtained here do not depend on the poorly known QSO triggering history, and we expect that these obtained constraints could be further used to infer the triggering history of seed BHs or refine the coevolution model for QSOs and galaxy spheroids (see also Blandford 2003).

## 5.2. Obscured QSOs/AGNs

Based on the assumption that the extragalactic X-ray background is mainly contributed by QSOs/AGNs, a larger number of obscured QSOs/AGNs (more than the optically bright or unobscured QSOs by a factor of  $\gtrsim 4$ ) were expected to exist from the X-ray background synthesis model (e.g., Gilli, Salvati & Hasinger 2001, and references therein). The existence of those sources is generally consistent with the expectation of the unification model of QSOs/AGNs (Antonucci 1993): if the dusty torus is along the line of sight, the light from these QSOs/AGNs will be absorbed by the dusty torus (this structure is proposed to explain the classification of Seyfert 1 and Seyfert 2 galaxies at low redshift  $z < 1$ ) and these QSOs/AGNs might be missed from observations in the optical band. In this scenario, obscuration is generally a geometric effect, and the obscured fraction is determined by the opening angle of the dusty torus. If the opening angle is the same for all QSOs/AGNs, the fraction of obscured QSOs/AGNs will be independent of the intrinsic luminosity of QSOs/AGNs.

Recent X-ray observations by Chandra and XMM-Newton confirm the existence of obscured AGNs/QSOs (e.g., Barger et al. 2003). However, the fraction of obscured QSOs/AGNs appears not constant, which is higher at low redshift ( $z \lesssim 1$ ) than at high redshifts ( $z \gtrsim 1.5$ ), and the obscured QSOs/AGNs have smaller BHs compared to optically bright QSOs (e.g., less than a few times  $10^8 M_{\odot}$ ; see a recent review by Fabian 2003 and references therein). This observational result contradicts with the expectation from the simple unification model if the opening angles of the torus are the same for all QSOs/AGNs, which might suggest that either the opening angle of the torus is smaller in luminous QSOs/AGNs than in faint QSOs/AGNs or QSOs/AGNs are obscured only at the early stage of their nuclear activities (Fabian 1999).

The relation between the local BHMF and the QSOLF established in this paper may provide a way to explore the underlying physics of the obscured QSOs/AGNs, independent of the X-ray background synthesis model. With the ongoing and future observations on obscured QSOs/AGNs (e.g., the X-ray deep surveys by XMM and Chandra), together with the observations on un-obscured QSOs/AGNs (e.g., by SDSS), we expect that more accurate constraints on QSO models, the BH growth, and the physical mechanism of the obscuration can be obtained, which will improve our understanding of the coevolution of QSOs and galaxy

spheroids.

### 5.3. BH mergers after the quenching of the nuclear activity and BH ejections

The effect of BH mergers on the local BH distribution function, which depends on the galaxy merger rate and the binary BH evolution process, is still very uncertain (e.g., Begelman, Blandford & Rees 1980; Yu 2002; Milosavljević & Merritt 2002; Volonteri, Haardt & Madau 2002). For simplicity, here we only discuss the effects of mergers after the quenching of the nuclear activity. Since mergers of small BHs form big BHs, BH mergers may make the BHMF increase at the high-mass end and decrease at the low-mass end. Thus, the time integral of the QSOLF predicted from the local BHMF (eq. 18) might be overestimated at the luminous end and underestimated at the faint end as a result of BH mergers. Indeed, the tentative result from the hierarchical galaxy formation scenario shown in Fig. 5 of Kauffmann & Haehnelt (2000) is that the BHMF at redshift 0 is lower than the BHMFs at higher redshifts (0.5, 1, 2) by a factor of  $< 2$  at BH mass  $\lesssim 10^{8.5-9} M_{\odot}$  and is higher than those BHMFs at higher redshifts at BH mass  $\gtrsim 10^{8.5-9} M_{\odot}$ . Thus, at least the models ruled out by applying inequalities (60) and (62) at the luminous end ( $M_B \sim -26$ ) without considering BH mergers will still be ruled out.

Not all massive BHs may reside in galactic centers (see § 3.2.1 in Yu & Tremaine 2002). For example, BHs may be ejected from galactic centers through either interactions of three or more BHs (e.g., Valtonen 1996) or gravitational radiation reaction during BH coalescence (Rees 2001), and BHs may also be left in galactic halos after galaxy mergers if the BH mass ratio of the two merging galaxies is small enough (e.g.,  $\lesssim 0.001$ ; Yu 2002). After considering the possibility that there might be some BHs that have experienced the QSO phases not locating in galactic centers, the time integral of the QSOLF predicted from local galaxies in this paper would increase. Currently, it is hard to give an estimate on the fraction of the BHs ejected from galactic centers or left in galactic halos during galaxy mergers by both theoretical models (also because both the BH and galaxy merger history and the BBH merger process are still very uncertain) and observations. Volonteri, Haardt & Madau (2002) study the assembly and merging history of massive BHs in the hierarchical models of galaxy formation and argue that the population of BHs wandering in galactic halos and the intergalactic medium at the present epoch contributes to the total BH mass density by  $\lesssim 10\%$ , which (if true) suggests that ignoring BH ejections would not significantly affect the results of this paper.

A complete and quantitative consideration of BH mergers or ejections is beyond the scope of this paper.

## 6. Other possible applications

In this section we discuss two possible applications of the work established in § 2, to the study of the demography of QSOs/AGNs and the demography of the hot stellar components of normal galaxies at intermediate redshift.

### 6.1. Demography of QSOs/AGNs

Consider such a galactic property  $\mathcal{V}$ , which does not significantly change during the nuclear active phase and after the quenching of the phase and is closely correlated with the BH mass  $M_{\text{BH},0}$  at present. Study of the relation between the BH mass and  $\mathcal{V}$  in QSOs/AGNs, as well as in nearby galaxies, might provide valuable

information on QSO models and BH growth. Below we show a way to investigate the relation between the BH mass and  $\mathcal{V}$  in QSOs/AGNs using the work in § 2.

The posterior distribution of  $M_{\text{BH},0}$  given the luminosity  $L$  of a QSO can be defined as follows:

$$\mathcal{P}(M_{\text{BH},0}|L) \equiv \frac{\int_0^{t_0} dt \int_0^t dt_i \mathcal{N}(t_i, M_{\text{BH},0}, L, t)}{\int_0^\infty dM_{\text{BH},0} \int_0^{t_0} dt \int_0^t dt_i \mathcal{N}(t_i, M_{\text{BH},0}, L, t)} = \frac{\tau_{\text{life}}(M_{\text{BH},0})P(L|M_{\text{BH},0})n_{M_{\text{BH}}}(M_{\text{BH},0}, t_0)}{\mathcal{T}_{L,\text{local}}(L, t_0)}, \quad (64)$$

where equations (17) and (18) are used. Thus, given the local BHMF and the luminosity evolution of individual QSOs  $\mathcal{L}(M_{\text{BH},0}, \tau)$ , which can be used to obtain  $\tau_{\text{life}}(M_{\text{BH},0})P(L|M_{\text{BH},0})$ , we may use equation (64) to get  $\mathcal{P}(M_{\text{BH},0}|L)$  and further use the local  $M_{\text{BH},0} - \mathcal{V}$  relation and get the distribution of  $\mathcal{V}$  at a given  $L$  or  $M_{\text{BH}}$  in QSOs. Comparison of future observation results (see also current observational results on the BH mass-velocity dispersion relation in QSOs by Shields et al. 2003) with the expected relations between the galactic parameter  $\mathcal{V}$  and the luminosity/BH mass of QSOs may further constrain the QSO luminosity evolution.

In a separate paper (Yu & Lu 2004) we will explore the nuclear luminosity/BH mass and velocity dispersion relation in QSOs/AGNs in the way described above, assuming that the velocity dispersion of the hot stellar components of galaxies does not significantly change during the nuclear active phase and after the quenching of the phase.

## 6.2. The distribution of velocity dispersions in elliptical galaxies and bulges of S0/spiral galaxies at intermediate redshift

Study of the demography of galaxies at all redshifts may help us understand the formation and evolution of galaxies. The past decade has seen dramatic expansion of the knowledge on intermediate- and high-redshift galaxies in both observations and theories, as well as on local galaxies, such as the observations of the Lyman-break galaxies at redshift  $z \sim 2 - 4$  (e.g., Adelberger et al. 2003), the semi-analytic hierarchical galaxy formation models to explain and predict the observational properties of both early-type and late-type galaxies (e.g., White & Frenk 1991; Kauffmann, White & Guiderdoni 1993; Cole et al. 1994, 2000), etc. Below using the work in § 2, we point out a simple way to estimate the velocity dispersion distribution in elliptical galaxies and the bulge components of S0/spiral galaxies at intermediate redshift ( $1 \lesssim z \lesssim 2.5$  here), which are still currently poorly known and are expensive and difficult to measure by observations.

We define  $n_{M_{\text{BH}}}(M_{\text{BH},0}, t)$  as the BHMF of dead QSOs at cosmic time  $t$  so that  $n_{M_{\text{BH}}}(M_{\text{BH},0}, t)dM_{\text{BH},0}$  represents the comoving number density of the BHs whose nuclear activities had been quenched before time  $t$  and the mass of these BHs is in the range  $M_{\text{BH},0} \rightarrow M_{\text{BH},0} + dM_{\text{BH},0}$  from the quenching time to the present time  $t_0$ . Similarly as the derivation to get equations (18) and (21), we have

$$\int_0^t \Psi_L(L, t) dt = \int_0^\infty dM_{\text{BH},0} \tau(M_{\text{BH},0}) P(L|M_{\text{BH},0}) n_{M_{\text{BH}}}(M_{\text{BH},0}, t), \quad (65)$$

as long as the condition

$$\int_0^t \Psi_L(L, t) dt \gg \int_{t-\tau_{\text{life}}}^t \Psi_L(L, t) dt \quad (66)$$

is satisfied. Condition (66) represents that most QSOs contributing to the integral of the QSOLF over the cosmic time  $0 - t$  have become quiescent (note the similarity to the necessary condition to hold eq. 18 in § 2

that most or all QSOs are quiescent at present time  $t_0$ ). Using the observed QSOLF shown in § 3.2, we find that condition (66) can be satisfied at redshift  $z \lesssim 2.5$  if  $\tau_{\text{life}} \lesssim 4\tau_{\text{Sp}}(\epsilon = 0.1) \simeq 2 \times 10^8 \text{ yr}$ .

As shown in § 4.2, the comparison between relation (21) and observations may provide constraints on the QSO luminosity evolution or  $\tau(M_{\text{BH},0})P(L|M_{\text{BH},0})$ . Given  $\tau(M_{\text{BH},0})P(L|M_{\text{BH},0})$  and the QSOLF,  $n_{M_{\text{BH}}}(M_{\text{BH},0}, t)$  can be uniquely determined from equation (65) (which is just a typical inverse problem). According to Bayes's theorem, the distribution of the velocity dispersion of the hot stellar components of local galaxies given a BH mass  $M_{\text{BH},0}$  is given by:

$$P(\sigma|M_{\text{BH},0}) = \frac{P(M_{\text{BH},0}|\sigma)n_{\sigma}(\sigma, t_0)}{n_{M_{\text{BH}}}(M_{\text{BH},0}, t_0)}. \quad (67)$$

We assume that the formation and the significant part of the evolution of bulges are simultaneous with the significant evolution (and/or formation) of their central BHs and that their velocity dispersions (and BH masses) do not significantly change after the quenching of the nuclei activity. Thus, there will be little evolution of the BH mass and velocity dispersion relation in those galaxies after they have experienced QSO phases, and the significant part of the evolution of the BH mass-velocity dispersion relation is recorded only in QSOs/AGNs. With  $P(\sigma|M_{\text{BH},0})$  obtained in equation (67), the velocity dispersion distribution of the hot stellar components of galaxies at low and intermediate redshift ( $z \lesssim 2.5$ ) can be given by

$$n_{\sigma}(\sigma, t) = \int_0^{\infty} dM_{\text{BH},0} P(\sigma|M_{\text{BH},0}) n_{M_{\text{BH}}}(M_{\text{BH},0}, t). \quad (68)$$

Note that according to the assumptions above, for normal galaxies, the hot stellar components exist only in those galaxies containing massive BHs (BH ejections are ignored here), and those galaxies that have experienced QSO phases and contain BHs must have hot stellar components, which of course should be tested by future observations. The methods above would still be applicable even if not all of the bulges or galaxies containing BHs follow these assumptions, but as long as most of them do. In addition, if the formation of the hot stellar components occurs before the formation of central BHs or the QSO phase (that is, some hot stellar components may not contain BHs), the velocity dispersion distribution of the galaxies obtained by the method in this section will at least give the lower limit to their realistic distribution.

## 7. Conclusions

Assuming that each massive BH in nearby galactic centers has experienced the QSO phase and becomes quiescent at present, we have established a relation between the QSOLF and the local BHMF by studying the continuity equation for the BH mass and nuclear luminosity distribution and ignoring BH mergers. This relation compares the time integral of the QSOLF and that inferred from the local BHMF and only incorporates the luminosity evolution of individual QSOs. The triggering history of the accretion onto seed BHs is (implicitly) considered in the continuity equation but is circumvented in the relation between the QSOLF and the local BHMF. For comparison, the old relations between QSOs and local BHs on the total/partial BH mass densities (see eqs. 26 and 29; Sołtan 1982; Yu & Tremaine 2002) include the effect of BH mergers, but the seed BH mass is ignored. The relation on the total BH mass density (eq. 26; Sołtan 1982) is unrelated with the luminosity evolution of individual QSOs, and the relation on the partial BH mass density (eq. 29; Yu & Tremaine 2002) assumes that the luminosity of QSOs is only an increasing function of their central BH mass (e.g., the Eddington luminosity in the calculation in Yu & Tremaine 2002). The new relation on the time integral of the QSOLF in this paper can be used to explore the luminosity evolution of individual QSOs (see § 1 and 2.3).



By applying observations into the relation established in this paper and assuming that the nuclear luminosity evolution includes two phases (first increasing at the Eddington luminosity with the BH growth and then declining), we find that the time integral of the QSOLF is generally consistent with that inferred from local BHs and obtain the following observational constraints on the QSO luminosity evolution and BH growth: (i) The QSO mass-to-energy efficiency  $\epsilon$  should be  $\gtrsim 0.1$  (see Fig. 4). (ii) The lifetime (defined directly through the luminosity evolution of individual QSOs) should be longer than  $\tau_{\text{Sp}} (\simeq 5 \times 10^7 \text{ yr})$  if  $\epsilon = 0.1$  and  $0.2\tau_{\text{Sp}} (\simeq 4 \times 10^7 \text{ yr})$  if  $\epsilon = 0.31$  (see Figs. 3 and 4). The characteristic declining timescale in the second phase should be significantly shorter than  $\tau_{\text{Sp}}$ , and BH growth should not be dominated by the second phase (when QSOs are accreting at sub-Eddington luminosities; see Fig. 6). (iii) The upper limit of the ratio of obscured QSOs/AGNs to optically bright QSOs is provided, which should be not larger than 7 at  $M_B \sim -23$  and 3 at  $M_B \sim -26$  if  $\epsilon = 0.31$  and not larger than 1 at  $M_B \sim -23$  and negligible at  $M_B \sim -26$  if  $\epsilon = 0.1$  (see Figs. 3 and 4). (iv) It is unlikely that most QSOs are accreting at super-Eddington luminosities (see Fig. 7). The constraints above are obtained by assuming that the two accretion phases appear only once in the luminosity evolution, although this assumption is not required in the relation established in this paper. The possibility of more complicated accretion patterns deserves further investigation.

We find that if the QSO lifetime is longer than a certain value (e.g.,  $\sim 4\tau_{\text{Sp}}$ ; see Fig. 3), the time integral of the nuclear LF inferred from local BHs becomes insensitive to the value of the QSO lifetime, and thus it is difficult to provide an accurate estimate on the QSO lifetime unless observations extend to fainter luminosities or precise measurements of the QSOLF and local BHMF are available (e.g., with error much less than 10%). We also point out that this difficulty would also exist in many other methods to estimate the QSO lifetime by using the QSOLF, as a result of the sharp decrease of the QSOLF at the bright end and the limited luminosity range in observations.

We show the importance of accurately measuring the intrinsic scatter in the relation between the BH mass and velocity dispersion of local galaxies and the scatter in the distribution of bolometric corrections of QSOs to precise understanding of the physics behind the QSO phenomenon and BH growth. Both of the scatters affect the shape and values of the time-integral of the nuclear LF, especially at the bright end.

With the upcoming more precise measurement on QSOs (including both unobscured and obscured AGNs) and the demography of local BHs and galaxies (by SDSS, Chandra, XMM, etc.), the method presented in this study would help to further explore the nuclear activity triggering and quenching mechanisms, obscuration of QSOs/AGNs, the demography of QSOs/AGNs, and the demography of normal galaxies at intermediate redshift and finally understand the physics behind the QSO phenomenon and the formation and evolution of galaxies.

We thank Ravi Sheth for helpful communication on the velocity dispersion distribution of nearby galaxies. We thank Norm Murray for helpful discussions. We thank the referee and Scott Tremaine for thoughtful comments.

## REFERENCES

- Adelberger, K. L., Steidel, C. C.; Shapley, A. E., Pettini, M. 2003, *ApJ*, 584, 45
- Aller, M. C., & Richstone, D. 2002, *AJ*, 124, 3035
- Antonucci, R. 1993, *ARA&A*, 31, 473

- Baes, M., Buyle, P., Hau, G.K.T., & Dejonghe, H. 2003, MNRAS, 341, L44
- Barger, A. J., Cowie, L. L., Capak, P., Alexander, D. M., Bauer, F. E., Fernandez, E., Brandt, W. N., Garmire, G. P., Hornschemeier, A. E. 2003, AJ in press, astro-ph/0306212
- Begelman, M. C. 2002, ApJ, 568, 97
- Begelman, M. C., Blandford, R. D., & Rees, M. J. 1980, Nature, 287, 307
- Bernardi, M., et al. 2003, AJ, 125, 1849
- Blandford, R. D. 2003, Carnegie Observatories Astrophysics Series, Vol. 1: Coevolution of Black Holes and Galaxies, ed. L. C. Ho (Cambridge: Cambridge Univ. Press)
- Blanton, M., et al. 2003, ApJ, 592, 812
- Boyle, B. J., Shanks, T., Croom, S. M., Smith, R. J., Miller, L., Loaring, N., & Heymans, C. 2000, MNRAS, 317, 1014
- Caditz, D., & Petrosian, V. 1990, ApJ, 357, 326
- Cavaliere, A., Morrison, P., & Wood, K. 1971, ApJ, 170, 223
- Cavaliere, A., Padovani, P. 1989, ApJ, 340, L5
- Chokshi, A., & Turner, E. L. 1992, MNRAS, 259, 421
- Cole, S., Aragon-Salamanca, A., Frenk, C. S., Navarro, J. F., & Zepf, S. E. 1994, MNRAS, 271, 781
- Cole, S., Lacey, C. G., Baugh, C., & Frenk, C. S. 2000, MNRAS, 319, 168
- Elvis, M., Risaliti, G., & Zamorani, G. 2002, ApJ, L75
- Elvis, M., Wilkes, B. J., McDowell, J. C., Green, R. F., Bechtold, J., Willner, S. P., Oey, M. S., Polonski, E., & Cutri, R. 1994, ApJS, 95, 1
- Fabian, A. C. 1999, MNRAS, 308, L39
- Fabian, A. C. 2003, Carnegie Observatories Astrophysics Series, Vol. 1: Coevolution of Black Holes and Galaxies, ed. L. C. Ho (Cambridge: Cambridge Univ. Press)
- Fabian, A. C., & Iwasawa, K. 1999, MNRAS, 303, 34
- Fan, X., et al. 2001, AJ, 121, 54
- Fan, X., et al. 2003, AJ, 125, 1649
- Ferrarese, L. 2002, ApJ, 578, 90
- Ferrarese, L., & Merritt, D. 2000, ApJ, 539, L9
- Ferrarese, L., Pogge, R. W., Peterson, B. M., Merritt, D., Wandel, A., & Joseph, C. L. 2001, ApJ, 555, L79
- Gebhardt, K., et al. 2000, ApJ, 539, L13
- Gebhardt, K., et al. 2003, ApJ, 583, 92

- Gilli, R., Salvati, M., & Hasinger, G. 2001, *A&A*, 366, 407
- Giovanelli, R., Haynes, M. P., Herter, T., Vogt, N. P., da Costa, L. N., Freudling, W., Salzer, J. J., & Wegner, G. 1997, *AJ*, 113, 53
- Haehnelt, M. G., Natarajan, P., & Rees, M. J. 1998, *MNRAS*, 300, 817
- Haiman, Z., & Hui, L. 2001, *ApJ*, 547, 27
- Haiman, Z., & Loeb, A. 1998, *ApJ*, 503, 505
- Haiman, Z., Ciotti, L., & Ostriker, J. P. 2003, *astro-ph/0304129*
- Hartwick, F.D.A., & Schade, D. 1990, *ARA&A*, 28, 437
- Hewett, P. C., Foltz, C. B., & Chaffee, F. H. 1995, *AJ*, 109, 1498
- Kauffmann, G., & Haehnelt, M. 2000, *MNRAS*, 311, 576
- Kauffmann, G., White, S.D.M., & Guiderdoni, B. 1993, *MNRAS*, 264, 201
- Kormendy, J. 2003, *Carnegie Observatories Astrophysics Series*, Vol. 1: Coevolution of Black Holes and Galaxies, ed. L. C. Ho (Cambridge: Cambridge Univ. Press)
- Kormendy, J., & Gebhardt, K. 2001, in Wheeler, J. C., , Martel, H., eds, *AIP Conf. Proc. Vol. 586*, 20th Texas Symposium On Relativistic Astrophysics. Am. Inst. Phys., New York, p. 363, *astro-ph/0105230*
- Kormendy, J., & Richstone, D. 1995, *ARA&A*, 33, 581
- Li, L.-X., & Paczyński, B. 2000, *ApJ*, 534, L197
- Lynden-Bell, D. 1969, *Nature*, 223, 690
- Magorrian, J., et al. 1998, *AJ*, 115, 2285
- Marconi, A., & Salvati, M. 2002, in *ASP Conf. Ser. 258*, Issues in Unification of Active Galactic Nuclei, ed. R. Maiolino, A. Marconi, & N. Nagar (San Francisco: ASP), 217
- Martini, P. 2003, *Carnegie Observatories Astrophysics Series*, Vol. 1: Coevolution of Black Holes and Galaxies, ed. L. C. Ho (Cambridge: Cambridge Univ. Press)
- Martini, P., & Weinberg, D. H. 2001, *ApJ*, 547, 12
- Merritt, D., & Ferrarese, L. 2001, *ApJ*, 547, 140
- Milosavljević, M., & Merritt, D. 2002, *astro-ph/0212459*
- Narayan, R., Igumenshchev, I. V., & Abramowicz, M. A. 2003, *astro-ph/0305029*
- Narayan, R., & Yi, I. 1994, *ApJ*, 428, L13
- Pei, Y. C. 1995, *ApJ*, 438, 623
- Rees, M. J. 1984, *ARA&A*, 22, 471

- Rees, M. J. 2001, in *Black Holes in Binaries and Galactic Nuclei*, Proceedings of the ESO Workshop held at Garching, Germany, 6-8 September 1999, ed. L. Kaper, E. P. J. van den Heuvel, & P. A. Woudt, p.351 (Germany: Springer)
- Salpeter, E. E. 1964, ApJ, 140, 796
- Salucci, P., Szuszkiewicz, E., Monaco, P., & Danese, L. 1999, MNRAS, 307, 637
- Shaver, P. A., Wall, J. V., Kellermann, K. I., Jackson, C. A., & Hawkins, M.R.S. 1996, Nature, 384, 439
- Sheth, R. K., et al. 2003, ApJ, 594, 225
- Shields, G. A., Gebhardt, K., Salviander, S., Wills, B. J., Xie, B., Brotherton, M. S., Yuan, J., & Dietrich, M. 2003, ApJ, 583, 124
- Small, T. A., & Blandford, R. D. 1992, MNRAS, 259, 725
- Sołtan, A. 1982, MNRAS, 200, 115
- Thorne, K. S. 1974, ApJ, 191, 507
- Tremaine, S., et al. 2002, ApJ, 574, 740
- Valtonen, M. J. 1996, MNRAS, 278, 186
- Volonteri, M., Haardt, F., & Madau, P. 2002, Ap&SS, 281, 501
- Wang, L., Caldwell, R. R., Ostriker, J. P., Steinhardt, P. J. 2000, ApJ, 530, 17
- Warren, S. J., Hewett, P. C., & Osmer, P. S. 1994, ApJ, 421, 412
- White, S.D.M., & Frenk, C. S. 1991, ApJ, 379, 52
- Yu, Q. 2002, MNRAS, 331, 935
- Yu, Q., & Lu, Y. 2004, ApJ, 610, 93
- Yu, Q., & Tremaine, S. 2002, MNRAS, 335, 965
- Zel’dovich, Ya. B., & Novikov, I. D. 1964, Sov. Phys. Dokl., 158, 811